

Università degli Studi di Napoli “Federico II”



**SCUOLA POLITECNICA E DELLE SCIENZE DI BASE
DIPARTIMENTO DI INGEGNERIA INDUSTRIALE**

**CORSO DI LAUREA IN INGEGNERIA AEROSPAZIALE
CLASSE DELLE LAUREE IN INGEGNERIA INDUSTRIALE (L-9)**

Elaborato di laurea in Meccanica del Volo
**Propulsive effects on the stability and control
characteristics of an innovative 19-pax aircraft
model**

**Relatore:
Prof. Danilo Ciliberti**

**Candidato:
Maria Perfetto
Matr. N35003796**

ANNO ACCADEMICO 2022 – 2023

*“Alla tua testa dura,
all’ansia e alla paura,
giuro che un po’ mi fa ridere.”
- ‘Ridere’, Pinguini Tattici Nucleari*

Abstract

The purpose of this work is to evaluate propulsive effects on the stability and control characteristics of an aircraft, the PROSIB 19 pax with the implementation of propellers as actuator disks on OpenVSP. This one is an open-source parametric aircraft geometry tool originally developed by NASA. Then the analysis is done using VSPAERO, a fast and linear solver that models the leading surface by assimilating them to an infinitely thin sheet of discrete vortices that are applied to each panel generated in OpenVSP file and then evaluated over the entire surface. Then a comparison between the results of propellers off-analysis and propellers on-analysis is made to evaluate advantages and disadvantages of DEP (distributed electric propulsion). DEP is an innovative aircraft design concept that has the potential to improve aircraft performance using electrically powered propulsor unit, which can be, for example, propellers that can provide thrust directly or may be used as an aerodynamic enhancement device.

Sommario

Lo scopo di questo lavoro è la valutazione degli effetti propulsivi sulla stabilità e sul controllo di un modello di velivolo, il PROSIB 19 pax con l'implemento delle eliche come dischi attuatori su OpenVSP. Quest'ultimo è uno strumento di geometria aeronautica parametrica open source originariamente sviluppato dalla NASA. L'analisi è eseguita utilizzando VSPAERO, un solutore veloce e lineare che modella le superfici portanti assimilandole ad un foglio infinitamente sottile di vortici discreti che poi vengono applicati a ciascun pannello del file della geometria di OpenVSP e valutati sull'intera superficie. Viene poi effettuato un confronto tra i risultati ottenuti senza le eliche e con le eliche attive, per valutare i vantaggi e gli svantaggi della DEP (propulsione elettrica distribuita). La DEP rappresenta un concetto di design innovativo che ha le potenzialità per aumentare le performance di un velivolo, attraverso unità propulsive alimentate elettricamente, che possono essere ad esempio le eliche che forniscono spinta in modo diretto o possono essere usate come dispositivi di miglioramento aerodinamico.

Table of contents

1. Introduction	7
1.1 Objectives	7
1.2 Layout of the work.....	7
2. Theoretical background.....	8
2.1 Actuator disk theory.....	8
2.2 DEP technology	10
2.3 VLM.....	11
3. Design of the project	15
3.1 OpenVSP	15
3.2 VSPAERO	16
3.3 Geometric model.....	17
4. Results and discussion.....	22
4.1 Wing.....	22
4.2 Wing and Horizontal tail.....	24
4.3 Complete aircraft	24
4.4 Aircraft component comparison curves	24
4.5 Wing with different grid	27
4.6 Complete aircraft with different grid	29
4.7 Flap effects.....	31
4.8 Elevator effects	34
4.9 Prop on- Prop off comparison.....	41
5. Conclusions	44

List of figure

Figure 2. 1 Velocity and static pressure distribution due to momentum theory.....	8
Figure 2. 2 Three Different Implementations of DEP Technology	11
Figure 2. 3 Analysis of the profile	13
Figure 2. 4 Vortex filament	14
.....	
Figure 3. 1 OpenVSP: selection of component	15
Figure 3. 2 VSPAERO interface	16
Figure 3. 3 PROSIB 19 pax- wing with DEP	17
Figure 3. 4 PropGeom interface	18
Figure 3. 5 Propeller placement.....	19
Figure 3. 6 Aircraft right-iso view.....	19
Figure 3. 7 VSPAERO: disk details	20
Figure 3. 8 VSPAERO advanced settings	21
.....	
Figure 4. 1 Wing section 1	22
Figure 4. 2 Wing section 2	22
Figure 4. 3 VSPAERO overview panel.....	23
Figure 4. 4 CL- α comparison curves	25
Figure 4. 5 CM γ - α comparison curves	25
Figure 4. 6 CL/CD comparison curves.....	26
Figure 4. 7 CL-CD comparison curves.....	26
Figure 4. 8 Wing section 1 (new grid).....	27
Figure 4. 9 Wing section 2 (new grid).....	27
Figure 4. 10 CL- α comparison curves	28
Figure 4. 11 CM γ - α comparison curves	28
Figure 4. 12 CL/CD- α comparison curves	29
Figure 4. 13 CL-CD comparison curves.....	29
Figure 4. 14 VSP viewer: $\alpha=0$	30
Figure 4. 15 VSP viewer: $\alpha = 10$	30
Figure 4. 16 $\alpha=10$ details	31

Figure 4. 17 Wakes with actuator disk model	31
Figure 4. 18 Flap panel	32
Figure 4. 19 CL- α deflections effects comparison plot	32
Figure 4. 20 CM γ - α deflections effects comparison plot	32
Figure 4. 21 CL/CD- α deflections effects comparison plot	33
Figure 4. 22 CL-CD deflections effects comparison plot.....	33
Figure 4. 23 Load distribution for various angles of attack.....	34
Figure 4. 24 FLAP and ELEVATOR panel	34
Figure 4. 25 Control Grouping section.....	35
Figure 4. 26 CL- α at different deflection of elevator	35
Figure 4. 27 CM γ - α at different deflection of elevator	36
Figure 4. 28 CL/CD- α at different deflection of elevator.....	36
Figure 4. 29 CL-CD at different deflection of elevator	37
Figure 4. 30 CL- α at different deflection of elevator	37
Figure 4. 31 CM γ - α at different deflection of elevator	38
Figure 4. 32 CL/CD- α at different deflection of elevator.....	38
Figure 4. 33 CL-CD at different deflection of elevator	39
Figure 4. 34 CL- α at different deflection of elevator	39
Figure 4. 35 CM γ - α at different deflection of elevator	40
Figure 4. 36 CL/CD- α at different deflection of elevator.....	40
Figure 4. 37 CL-CD at different deflection of elevator	41
Figure 4. 38 CL- α comparison plot	41
Figure 4. 39 CM γ - α comparison plot	42
Figure 4. 40 CL/CD- α comparison plot.....	42
Figure 4. 41 CL-CD comparison plot.....	43
Figure 4. 42 Load distribution comparison	44

List of tables

Table 3. 1 THERM Propeller Requirements	18
Table 3. 2 DEP Propeller Requirements.....	18
Table 3. 3 Input Data	20
.....	
Table 4. 1 Wing tables of coefficient	23
Table 4. 2 Wing and Horizontal tail tables of coefficient	24
Table 4. 3 Complete aircraft tables of coefficient	24
Table 4. 4 Wing tables coefficients (new grid)	27
Table 4. 5 Complete aircraft tables of coefficient (new grid)	30

1. Introduction

1.1 Objectives

The objective of this thesis is the valuation of propulsive effects on PROSIB 19 pax with the implementation of 10 propellers. The first step is modelling these propellers on OpenVSP as actuator disks, then the analysis is done in VSPAERO by entering different parameters related to the geometry of the aircraft, particularly of the propellers, which are of two different types. The results of the analyses were reported in graphs obtained with Microsoft Excel and related to the lift coefficient, moment coefficient obtained as the angle of attack varies, the drag polar curves and aerodynamic loads distribution. Then this work shows the same analyses but with a different grid to see if the results are different. These analyses were repeated for isolated wing, partial aircraft and total aircraft and for different deflection of flaps and elevator. In the end, a comparison is made between propellers on and propellers off (same aircraft).

1.2 Layout of the work

Chapter 2: This chapter deals with the theoretical foundations of actuator disk theory, DEP technology and VLM methods.

Chapter 3: This chapter introduces the geometry of propellers, OpenVSP and the VSPAERO setup.

Chapter 4: This chapter shows the data collected through the analyses and related graphs, tables and comparison.

Chapter 5: Conclusion chapter.

2. Theoretical background

2.1 Actuator disk theory

Actuator disk theory is also called Momentum Theory and is based on the idea to apply the basic conservation laws of fluid mechanics (conservation of mass, momentum and energy) to the rotor and flows to estimate the rotor performance. The momentum theory is characterized by the fact that the rotor is modeled as an actuator disk, which is a circular surface of zero thickness that is characterized by a pressure jump and that accelerates the air through the disk. Naturally, the actuator disk model is only approximating the rotor. The theory is based on the following assumptions:

- The disk is assumed to be very small thickness and has no mass, with only a frontal area.
- The air is an incompressible and inviscid fluid.
- The flow is uniform.
- The propeller produces a pressure jump across the disk equal to thrust per unit area of the disk.

Since the disk adds mechanical energy to the flow which passes through it, the velocity far behind the propeller will become larger than freestream. Because of the increase in energy of the flow just behind the propeller, the pressure will be greater than ambient, but the velocity will be the same as just in front of the disk. Far behind the disk, in the wake, the pressure will return to ambient pressure.

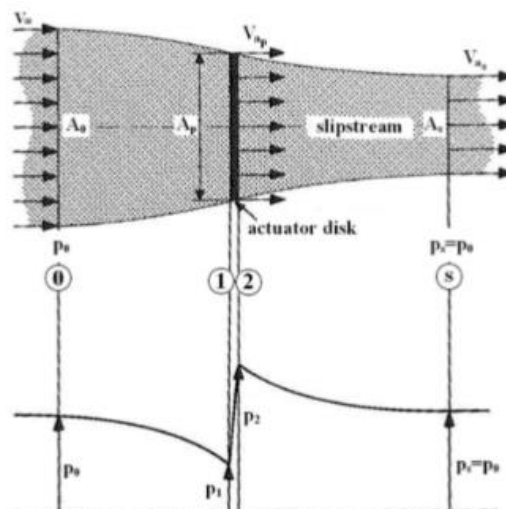


Figure 2. 1 Velocity and static pressure distribution due to momentum theory

The thrust of the propeller is:

$$T = \rho V_{as} A_s (V_{as} - V_{\infty}) \quad (2.1)$$

V_{as} is the velocity far downstream, where the pressure has returned to the ambient pressure.

A_s is the cross-sectional area of the slipstream.

Thrust is also equal to the pressure change through the disk:

$$T = A_p (p_2 - p_1) = A_p \Delta p \quad (2.2)$$

Then, applying Bernoulli equation upstream of the disk:

$$p_0 + \frac{1}{2} \rho V_{\infty}^2 = p_1 + \frac{1}{2} \rho V_{ap}^2 \quad (2.3)$$

While downstream:

$$p_2 + \frac{1}{2} \rho V_{ap}^2 = p_0 + \frac{1}{2} \rho V_{as}^2 \quad (2.4)$$

By subtracting the last two equation, we obtain the pressure jump:

$$\Delta p = \frac{1}{2} \rho (V_{as}^2 - V_{\infty}^2) \quad (2.5)$$

By replacing this equation in the thrust equation, we have:

$$T = A_p \frac{1}{2} \rho (V_{as}^2 - V_{\infty}^2) \quad (2.6)$$

The continuity equation is:

$$V_{ap} A_p = V_{as} A_s \quad (2.7)$$

Combining all the equation, we obtain:

$$V_{ap} = \frac{1}{2} (V_{\infty} + V_{as}) \quad (2.8)$$

This equation shows that the axial velocity at the actuator disk is the arithmetic mean of the axial freestream velocity and the axial slipstream velocity.

The propulsive efficiency is equal to:

$$\eta = \frac{2V_{\infty}}{V_{as} + V_{\infty}} \quad (2.9)$$

It's possible to write the propulsive efficiency as a function of the thrust:

$$T = 2\rho V_{ap} A_p (V_{ap} - V_\infty) \quad (2.10)$$

Solving this equation for V_{ap} :

$$V_{ap} = \frac{V_\infty}{2} + \sqrt{\frac{V_\infty^2}{4} + \frac{T}{2\rho A_p}} \quad (2.11)$$

Replacing the equation of the axial velocity into the equation of the propulsive efficiency leads to:

$$\eta = \frac{2}{1 + \sqrt{1 + \frac{T}{\frac{1}{2}\rho V_\infty^2 A_p}}} \quad (2.12)$$

It's important to underline that efficiency is only the theoretical upper limit since the axial momentum theory doesn't include any losses. One of the biggest limitations of the actuator disk theory is that it doesn't consider the design of individual propeller blades.

2.2 DEP technology

Distributed electric propulsion (DEP) systems use electrically driven propulsors which are only connected electrically to energy sources or power-generating devices. As a result, propulsors can be placed, sized, and operated with greater flexibility to provide improved performance over more traditional designs. The placement and configuration of propulsors can be used to mitigate the trailing vortex system of a lifting surface or leverage increases in dynamic pressure across blown surfaces for increased lift performance.

DEP systems are being proposed and developed for conventional, short, and vertical take-off and landing aircraft applications.

Additionally, DEP technology provides control capabilities of the vehicle dynamics, which could potentially lead to the elimination of more traditional control surfaces. Such a case would permit, for example, a reduction in the size or complete elimination of a vertical tail surface, resulting in a substantial reduction in aircraft weight.

Another benefit of DEP concepts is the possibility of reducing noise during take-off and landing phases of flight. In the turbofan systems currently used in large transport-class aircraft, the bypass ratio plays an important role in reducing such noise. For the case of a DEP concept, the effective bypass ratio, defined as the ratio of mass flow rate of all combined air flow entering the DEP fans over that entering the engine core, can be greatly increased by increasing the number of electrically driven fans. This approach significantly reduces the overall noise produced by the propulsion system, especially fan noise.

A concept that uses DEP is shown in Figure 2.1. Here, three different types of DEP are encountered. The propellers along the leading edge of the wing are used to enhance high-lift performance by increasing the dynamic pressure over the wing at low speeds, enabling a smaller wing. The propellers at the wingtips are used for primary propulsion, and rotate opposite of the wingtip vortex, increasing propulsive efficiency. The single small propeller at the aft end of the fuselage is used to accelerate the slow-moving air along the fuselage boundary layer to “cancel” out fuselage drag.

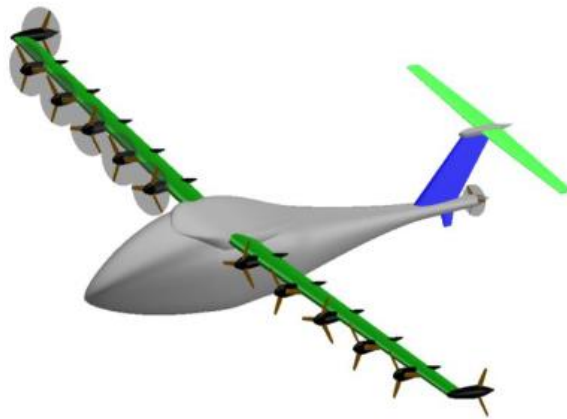


Figure 2. 2 Three Different Implementations of DEP Technology

One may object that if these four techniques can enable large performance benefits, then current aircraft would employ such strategies. The reasons for not utilizing such systems stems largely from the characteristics of conventional engines, is that this system is simply impractical to distribute many conventional engines due to their size and weight.

2.3 VLM

Vortex lattice methods (VLM) are numerical techniques used in aerodynamics to analyze and predict the behavior of aircraft, especially in the preliminary design phase. These methods

provide a relatively quick and computationally efficient way to estimate aerodynamic forces and moments acting on an aircraft. The aircraft geometry is divided into a set of lifting surfaces, such as wings and tail surfaces. It's important to note that while vortex lattice methods are valuable for quick estimations, they have limitations, particularly in capturing complex flow phenomena such as vortex breakdown or flow separation.

Let's suppose irrotational flow, which is defined as a flow where the vorticity ξ is equal to 0 at every point:

$$\xi = \nabla \times V = 0 \quad (2.13)$$

If we consider velocity potential, ϕ , as a scalar function, we have that:

$$\nabla \times (\nabla \phi) = 0 \quad (2.14)$$

Putting together the last two equations, it follows that:

$$V = \nabla \phi \quad (2.15)$$

Considering the principle of conservation of mass for an incompressible flow, we get that:

$$\nabla \cdot V = 0 \quad (2.16)$$

Combining the two previous formulas and we get:

$$\nabla \cdot (\nabla \phi) = 0 \text{ or } \nabla^2 \phi = 0 \quad (2.17)$$

This equation is the Laplace equation, that explains irrotational and incompressible flow. So, a complicated flow pattern for an irrotational and incompressible flow can be simplified by a series of elementary irrotational and incompressible flows. Vortex Lattice Method (VLM) is based on this line vortices.

The Vortex Lattice Method is based on the following assumptions: the lifting surfaces are thin. The influence of thickness on aerodynamic forces are neglected. Considering a symmetrical airfoil, the camber effect can also be neglected. After applying this boundary condition to Laplace's Equation, the problem can easily be solved by including the effect of angle of attack on a flat surface.

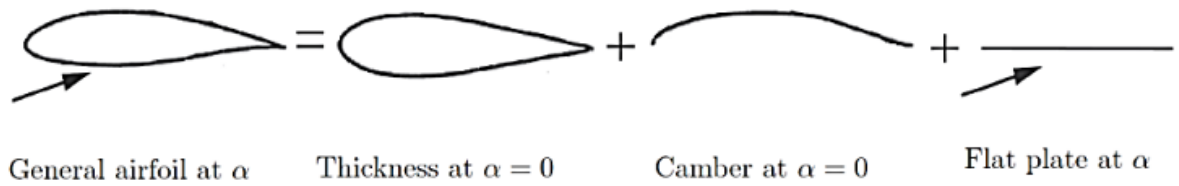


Figure 2. 3 Analysis of the profile

Considering a wing with a moderate angle of attack, the boundary condition states that normal flow across the thin wing's solid surface is zero. This means that also the velocity induced by the wing vortices from the wake is zero. In two dimensions, for a vortex line of infinite length, the induced velocity at a point is given by:

$$V_{\vartheta} = \frac{\Gamma}{2 \cdot \pi \cdot r} \quad (2.18)$$

Where Γ is the vortex circulation strength, r is the perpendicular distance between the point and the vortex line. The circulation has the same sign as its vorticity, so it is positive in the clockwise direction. The concept of point vortex can be extended to a general filament of three-dimensional vortex. The mathematical description of the flow induced by this filament is given by the Biot-Savart law. It states that the increment of the velocity dV at a point P due to a segment of a vortex filament dl at a point q is:

$$dV_p = \frac{\Gamma}{4\pi} \cdot \frac{dl \times r_{pq}}{|r_{pq}|^3} \quad (2.19)$$

This can then be integrated over the entire length of the vortex filament to obtain the induced velocity in point P:

$$V_p = \frac{\Gamma}{4\pi} \cdot \int \frac{dl \times r_{pq}}{|r_{pq}|^3} \quad (2.20)$$

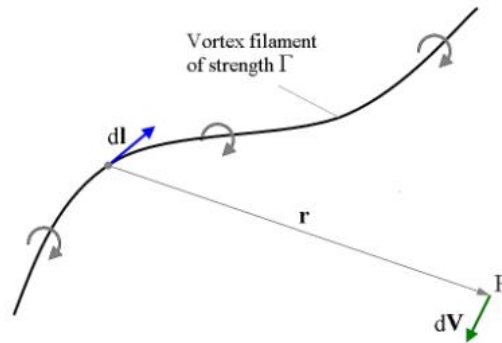


Figure 2. 4 Vortex filament

By applying principles such as the Kutta-Joukowski theorem, which relates the circulation around a lifting surface to the lift force, a system of linear equations is formed. These equations are typically solved iteratively to find the circulation distribution and, consequently, the aerodynamic forces on the aircraft. Once the circulation distribution is determined, aerodynamic coefficients such as lift, drag, and pitching moment can be calculated.

3. Design of the project

3.1 OpenVSP

OpenVSP (Open Vehicle Sketchpad) is an open-source parametric aircraft geometry tool originally developed by NASA. It can be used to create 3D models of aircraft and to support engineering analysis of those models. OpenVSP allows the user to quickly generate computer models from ideas, which can then be analyzed. As such, it is especially powerful in generating and evaluating unconventional design concepts.

In OpenVSP, the first step is the generation of the geometry: we can modify the parameters of every component by selecting them. It can be seen in Figure 3. 1:

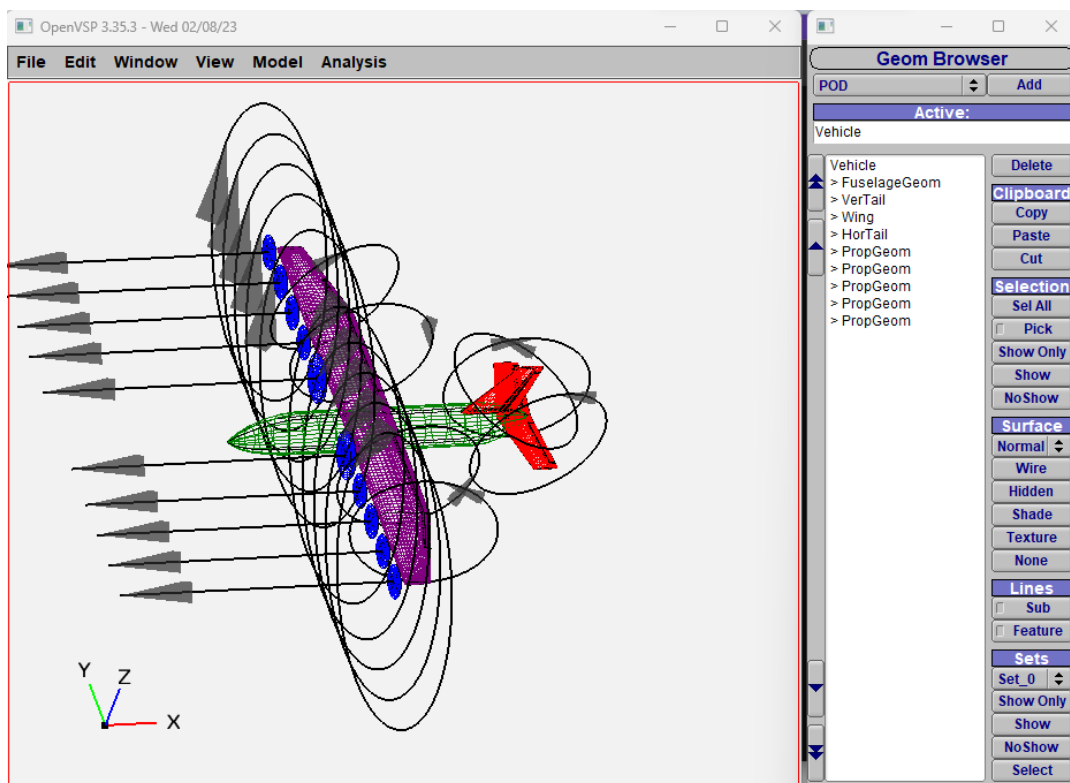


Figure 3. 1 OpenVSP: selection of component

Important is the setting of the U parameter of Spanwise, in the main panels. This parameter can be chosen for the total component and in the subsections (SECT in the geometry panel). This step will be very useful in the discussion we will do later (paragraphs 4.5-4.6).

3.2 VSPAERO

VSPAERO is a potential flow aerodynamics tool developed by Dave Kinney at NASA Ames. The solver was designed from the ground up to leverage OpenVSP geometries and the DegenGeom thin-surface representation.

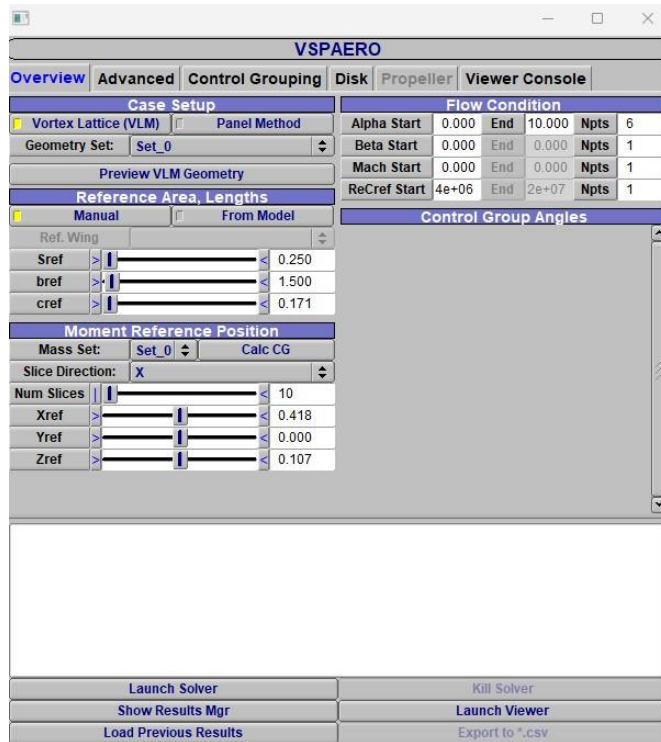


Figure 3. 2 VSPAERO interface

It is important to note that DegenGeom will write all the components in a model unless you specify a geometry set. The degenerate geometry files for your selected set of components are written from OpenVSP by choosing DegenGeom under the Analysis menu. The easiest way to generate a file for a new model is to open VSPAERO and once you select the Overview tab (Figure 3. 2), you'll find several different sliders and inputs that will help you define a Setup file. Once each value is defined for the flow conditions to be analyzed, click the Launch Solver button to automatically generate the Setup file and run VSPAERO. This software writes several types of files, below the ones that have been used in this work:

- LOD file, a representation of the local lift, drag and side force coefficient.
- POLAR file, where we can find the lift, drag and side force coefficient as a function of the input data.

3.3 Geometric model

This paragraph describes the aircraft geometry modeled with OpenVSP, particularly it will focus on the propeller's geometry and their operation. The aircraft design is shown in Figure 3.3:

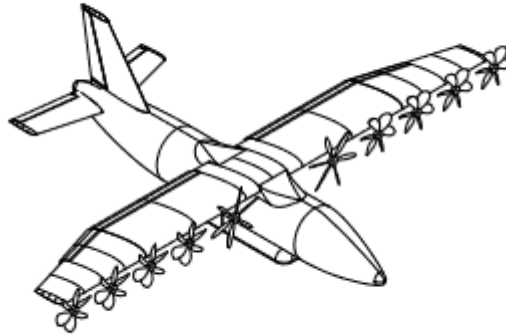


Figure 3.3 PROSIB 19 pax- wing with DEP

There are 10 propellers, 5 for each half of the wing. The project has 2 types of propellers:

- THERM, which are the bigger ones near the fuselage.
- DEP, which are the smaller ones, on the entire wing.

For their different sizes, they have different characteristics. For example, THERM propeller works at 8000 RPM, DEP propeller works at 10000 RPM. All the requirements of the THERM propellers are listed below:

DATA	VALUE	MEASURE UNIT
Nblades	6	-
Radius	0.0845	M
Hub_radius	0.01	M
Des_speed	35	m/s
RPM	8000	RPM
Thrust	3.5	Newton
Altitude	0	Km
cl	0.7	-

Table 3. 1 THERM Propeller Requirements

The THERM propeller design point will be at $J = \frac{V}{nD}$ equal to 1.5533, where V is the speed, n is the revolutions per seconds and D is the diameter.

In the table below, the requirements of DEP propeller:

DATA	VALUE	MEASURE UNIT
Nblades	6	-
Radius	0.0585	m
Hub_radius	0.01	m
Des_speed	35	m/s
RPM	10000	RPM
Thrust	4	Newton
Altitude	0	Km
cl	0.7	-

Table 3. 2 DEP Propeller Requirements

The DEP propeller operating point will be at $J = \frac{V}{nD}$ equal to 1.7949.

The actuator disk only requires in input the diameter of the disk for the geometry, because, as we said before, this model ignore the blades of the propeller. While for VSPAERO analyses, in input it requires the thrust coefficient (CT), power coefficient (CP) and rate per minute (RPM).

According to this geometry input data, we have to create disk on OpenVSP by selecting Propeller and choosing the option ‘Disk’ in the modeling panel, as in Figure 3. 4.

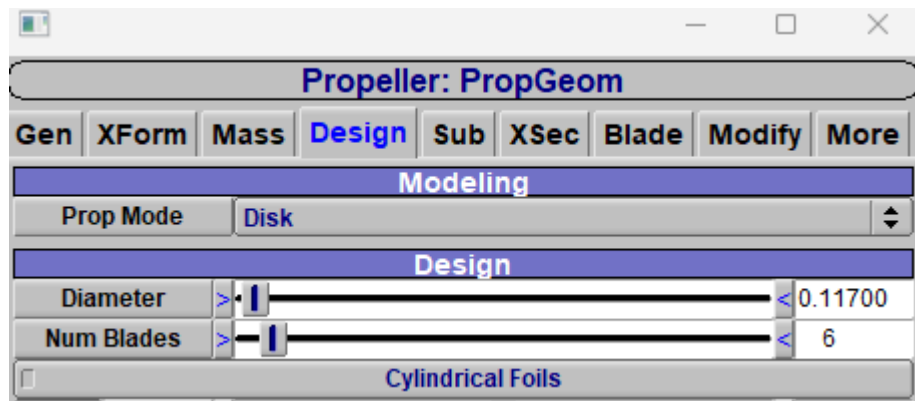


Figure 3. 4 PropGeom interface

Then we enter diameter and number of blades, even if this last parameter does not influence the geometry because we are not considering the option ‘blades’ in the section Prop Mode. Once we have created the geometry of the propellers, we must place them according to the right coordinates following the scheme in Figure 3. 5:

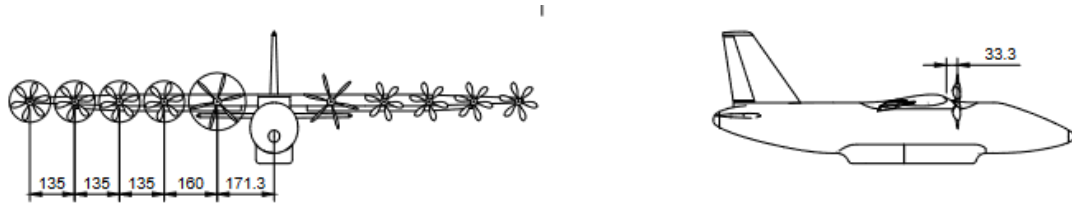


Figure 3. 5 Propeller placement

Once we have done the geometry and have set the right position on OpenVSP, we obtain:

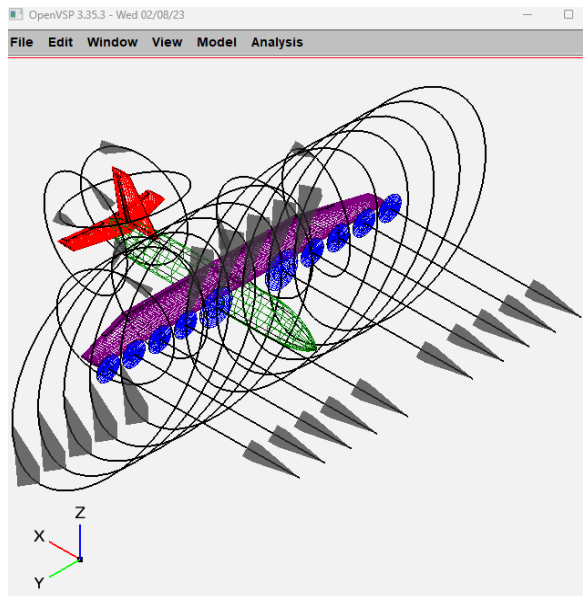


Figure 3. 6 Aircraft right-iso view

According to the operating points of both types of propellers, we can start to write the input file for the VSPAERO analysis:

INPUT DATA		
NAME	VALUE	UNITS
Sref	0.25	m ²
Cref	0.171	m
Bref	1.5	m
Xref	0.418	m
Yref	0	m
Zref	0.107	m
AoA(start)	0	deg

AoA(end)	10	deg
Beta	0	deg
Rho	1.225	kg/m ³
Vinf	35	m/s
Roll Rate	0	rad/s
Pitch Rate	0	rad/s
Yaw Rate	0	rad/s
DEP DISK DATA		
Diameter	0.117	m
Hub Dia.	0.02	m
rpm	10,000	RPM
CT	0.6262	-
CP	0.2773	-
J	1.7949	-
THERM DISK DATA		
Diameter	0.169	m
Hub Dia.	0.02	m
rpm	8,000	RPM
CT	0.1965	-
CP	0.0591	-
J	1.5533	-

Table 3. 3 Input Data

In the VSPAERO ‘Disk’ interface, we insert the data listed in Table 3. 3:

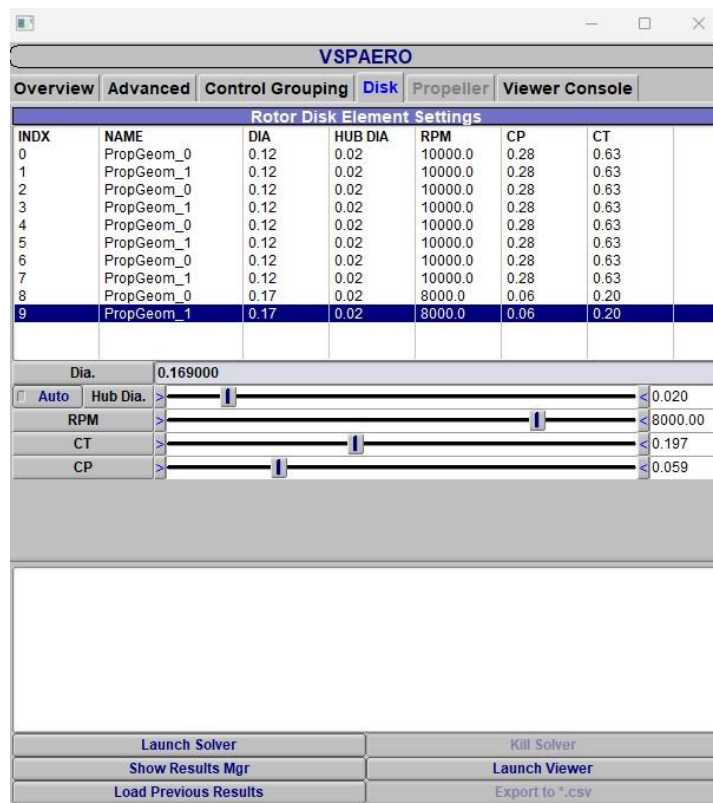


Figure 3. 7 VSPAERO: disk details

For each analysis, we must remember to select the option ‘Actuator disk’ in the Advanced options, as in Figure 3. 8.



Figure 3. 8 VSPAERO advanced settings

In this way, we can open the Disk panel, while selecting ‘Rotating blades’, we can modify the Propeller panel.

In the next chapter, we will see the results of the analyses with this input data.

4. Results and discussion

4.1 Wing

In this first part, we have done the analysis with a specific value for the grid set at $U = 18$, Rt. Cluster = 1.0 and Tip Cluster = 1.0 for the wing section 1 (Figure 4. 1) and $U = 12$, Rt. Cluster = 1.0 and Tip Cluster = 1.0 for wing section 2 (Figure 4. 2).

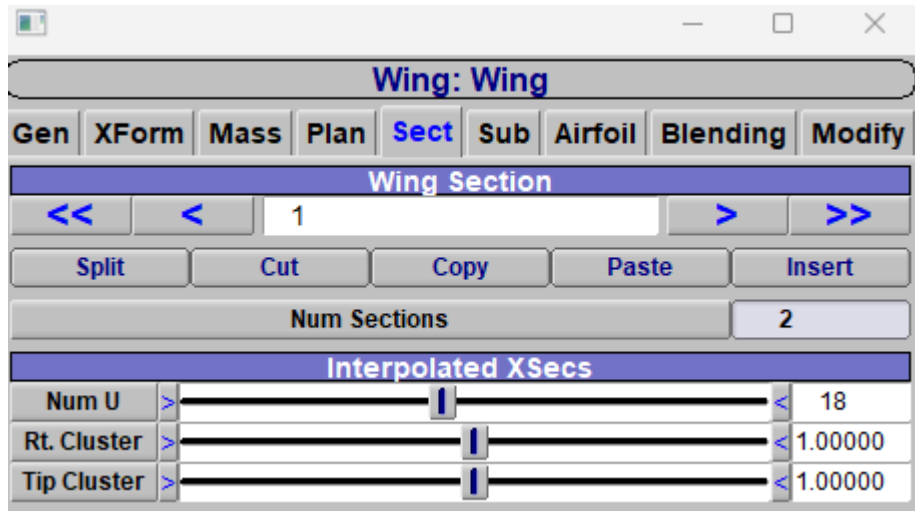


Figure 4. 1 Wing section 1

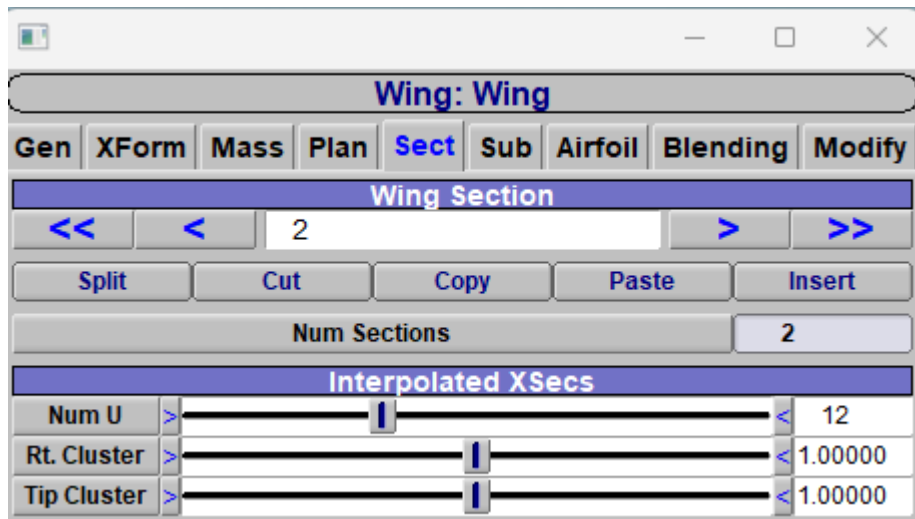


Figure 4. 2 Wing section 2

The analysis on VSPAERO is performed working on 6 different angles of attack from 0 to 10.

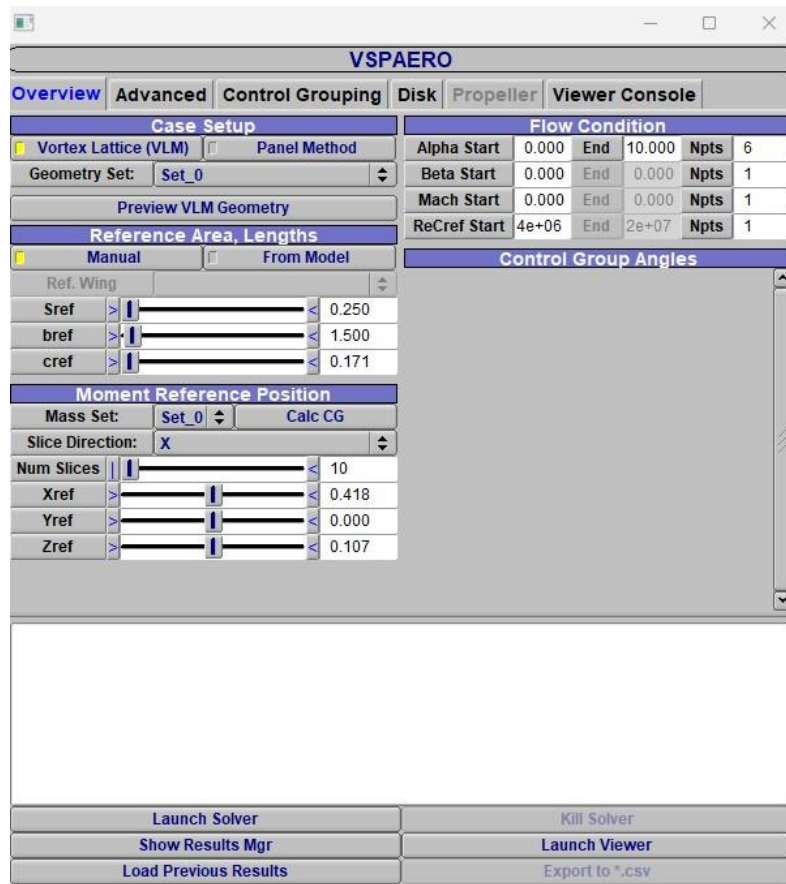


Figure 4. 3 VSPAERO overview panel

By selecting ‘SET 0’, as shown in Figure 4. 3, in which we entered only the wing with the propellers, it is possible to start the analysis, with the parameter set just as in figure.

So, we obtain these results:

AoA	CL	CDtot	CM_y	CL/CD
0.00000	0.10200	0.00815	-0.02200	12.51000
2.00000	0.28600	0.01110	-0.02900	25.77000
4.00000	0.48200	0.01780	-0.03800	27.08000
6.00000	0.66700	0.02740	-0.04000	24.34000
8.00000	0.85100	0.04020	-0.04200	21.17000
10.00000	1.03700	0.05620	-0.04300	18.45000

Table 4. 1 Wing tables of coefficient

4.2 Wing and Horizontal tail

By changing the set on the panel, we can proceed and do another analysis on a different set. In Table 4. 2, we can see the results of wing and horizontal tail together.

AoA	CL	CDtot	CMy	CL/CD
0.0000	0.0970	0.0099	-0.0090	9.7900
2.0000	0.2900	0.0132	-0.0698	21.9700
4.0000	0.5100	0.0207	-0.1360	24.6400
6.0000	0.7200	0.0318	-0.2030	22.6400
8.0000	0.9200	0.0470	-0.2660	19.5800
10.0000	1.1300	0.0650	-0.3400	17.3800

Table 4. 2 Wing and Horizontal tail tables of coefficient

4.3 Complete aircraft

Then we add the fuselage to another set and we have the results in Table 4. 3:

AoA	CL	CDtot	CMy	CL/CD
0.00000	0.09280	0.00977	0.00571	9.57000
2.00000	0.29500	0.01290	-0.04630	22.87000
4.00000	0.51000	0.02060	-0.10400	25.24000
6.00000	0.71400	0.03200	-0.15800	22.32000
8.00000	0.91800	0.04720	-0.21100	19.45000
10.00000	1.12000	0.06670	-0.26600	16.79000

Table 4. 3 Complete aircraft tables of coefficient

4.4 Aircraft component comparison curves

This section shows the aircraft component comparison curves of the aerodynamic coefficients, such as lift, moment and drag coefficients:

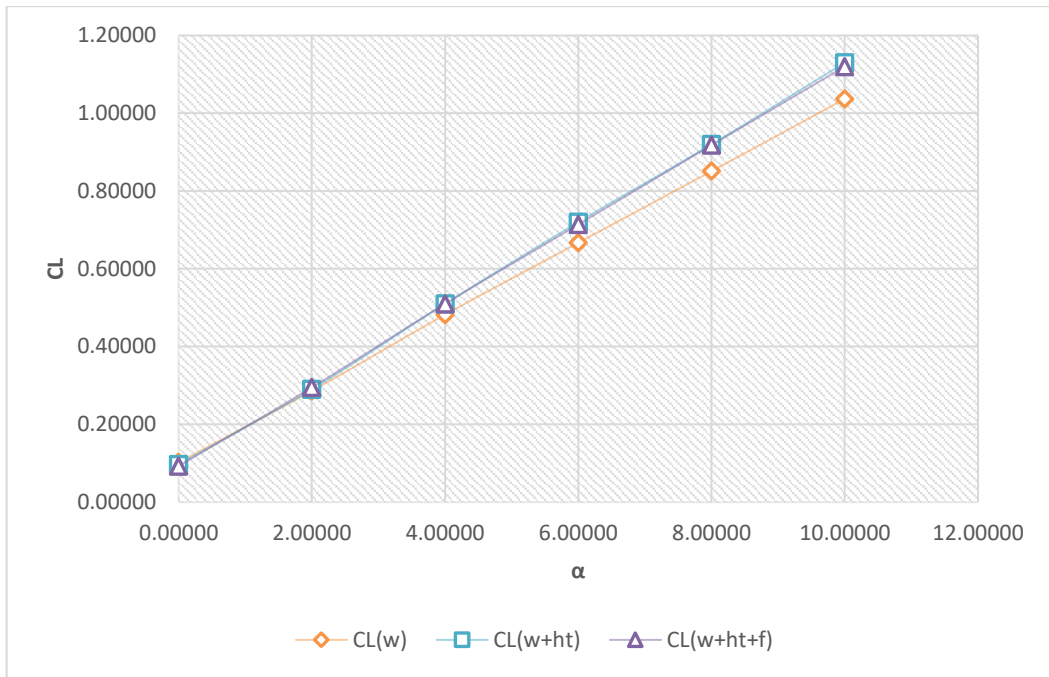


Figure 4. 4 CL- α comparison curves

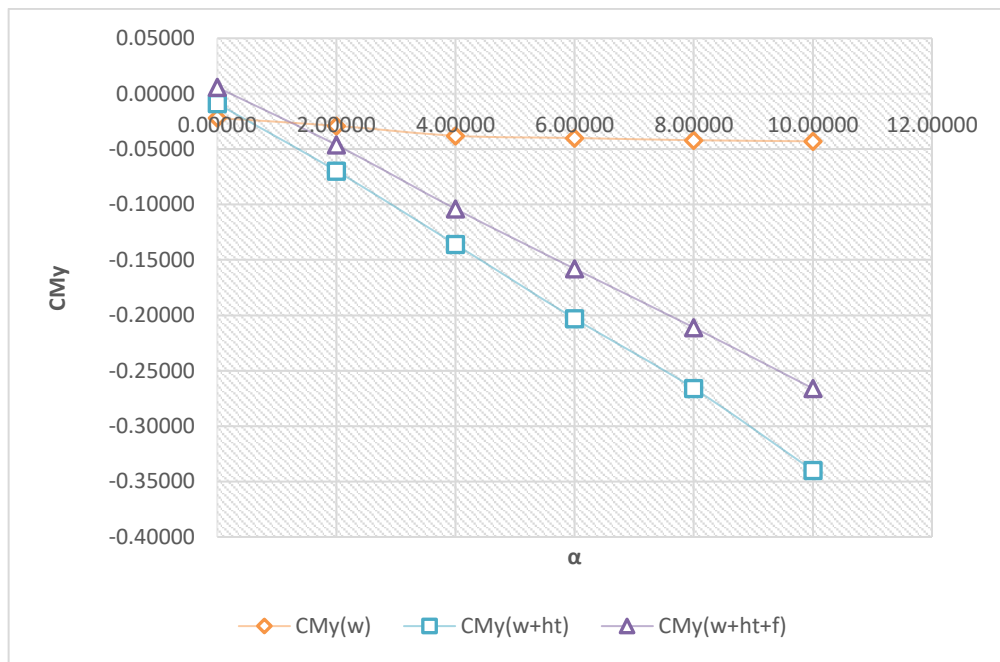


Figure 4. 5 CMY- α comparison curves

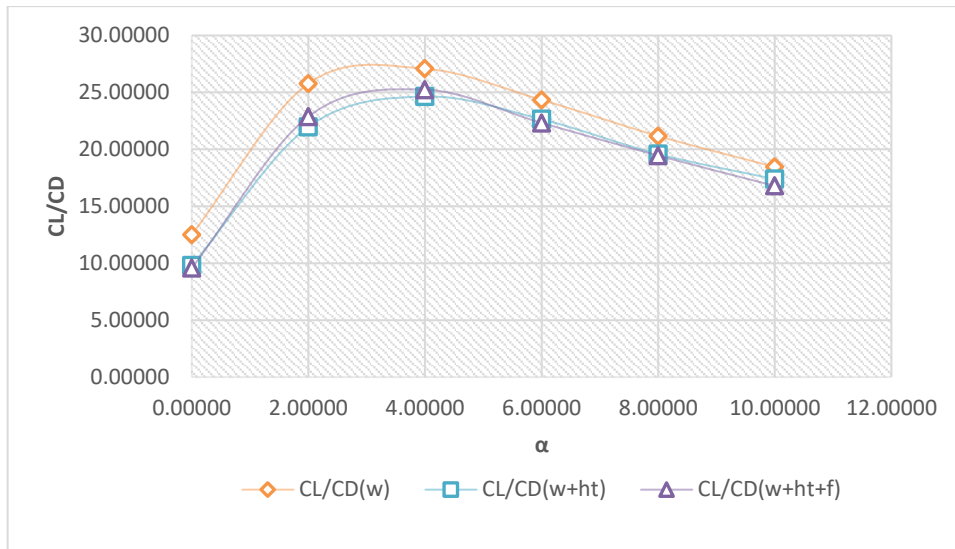


Figure 4. 6 CL/CD comparison curves

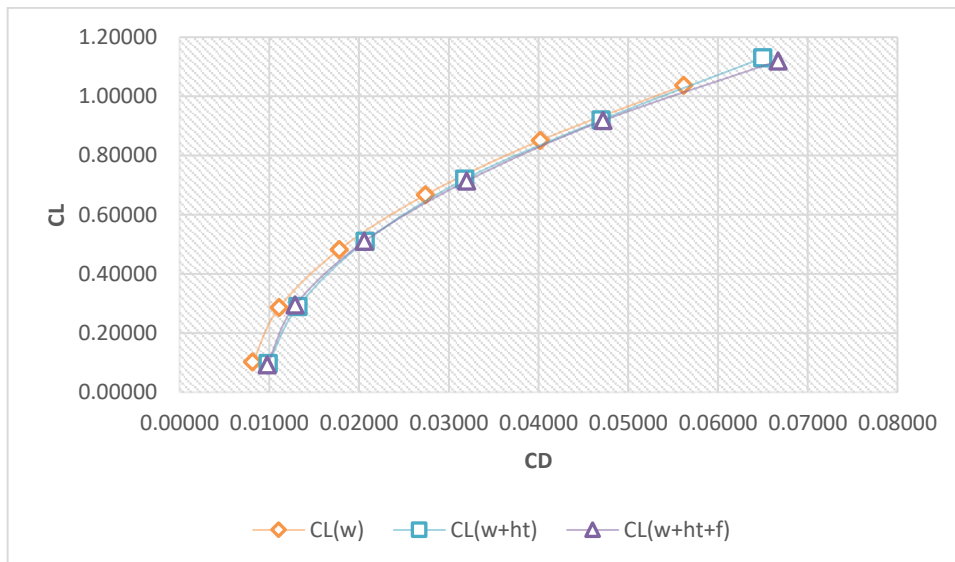


Figure 4. 7 CL-CD comparison curves

We can immediately see that adding Horizontal tail and fuselage, the $CL-\alpha$ curves (Figure 4. 4) increase the slope, this because we added surfaces, but the solver does not see the effect of the fuselage on the lift curve because it is very small compared to the effect of the wing, but it can be seen on the $CM_y-\alpha$ curve (Figure 4. 5). In addition, the effect of the fuselage has an importance on the CL/CD plot (Figure 4. 6) because it increases the induced drag and the curve moves downward.

All these results were plotted with flaps deflection at 0° .

4.5 Wing with different grid

In all the previous sections of these chapter, we have done the analysis with a certain grid. From now on, we change the grid of the wing sections and we see the difference:

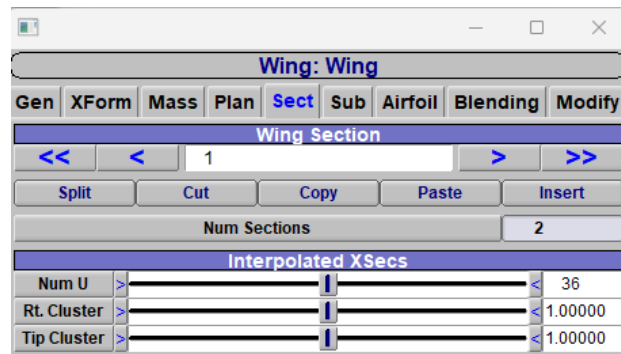


Figure 4. 8 Wing section 1 (new grid)

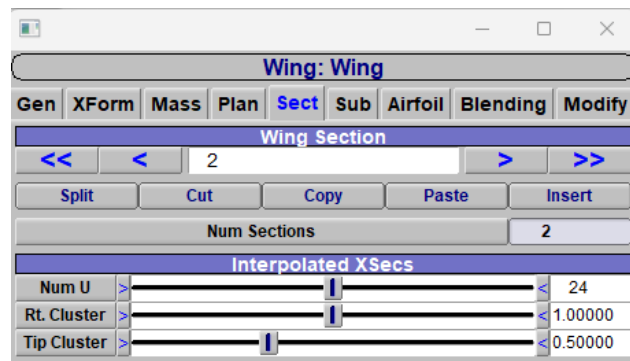


Figure 4. 9 Wing section 2 (new grid)

As it can be seen in Figure 4. 8 and Figure 4. 9, we changed Tip Cluster of wing section 2 from 1.0 to 0.5, and we have doubled up the Num U of both wing sections. So, by selecting 'Set 0', we obtain these coefficients:

AoA	CL	CDtot	CMy	CL/CD
0.00000	0.12828	0.00818	-0.02292	15.68852
2.00000	0.30682	0.01086	-0.02870	28.24372
4.00000	0.48668	0.01686	-0.03390	28.86816
6.00000	0.66422	0.02593	-0.03594	25.61410
8.00000	0.83368	0.03766	-0.03480	22.13527
10.00000	1.00792	0.05339	-0.03308	18.87966

Table 4. 4 Wing tables coefficients (new grid)

In this way, we can compare the 'old' grid with the new one (w' is the new one):

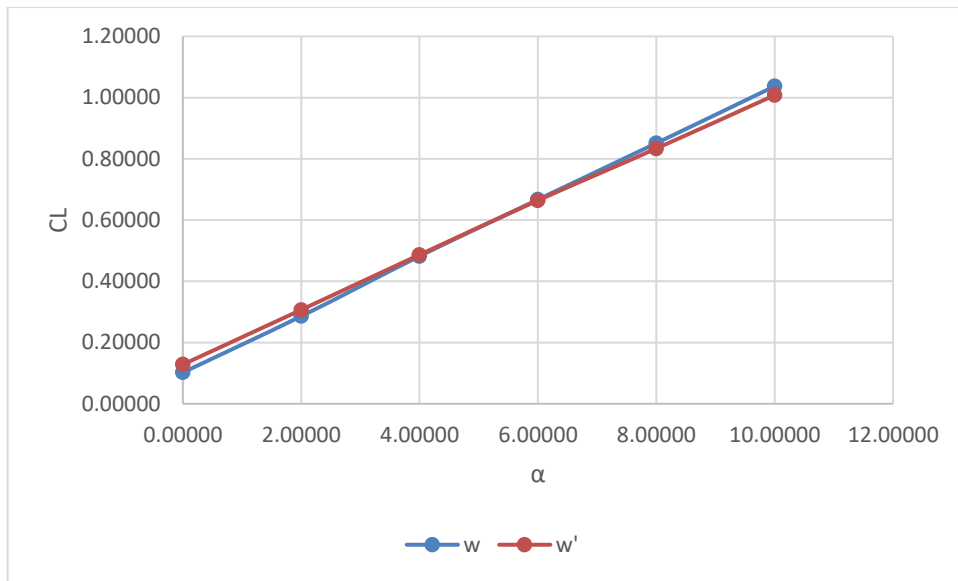


Figure 4. 10 CL- α comparison curves

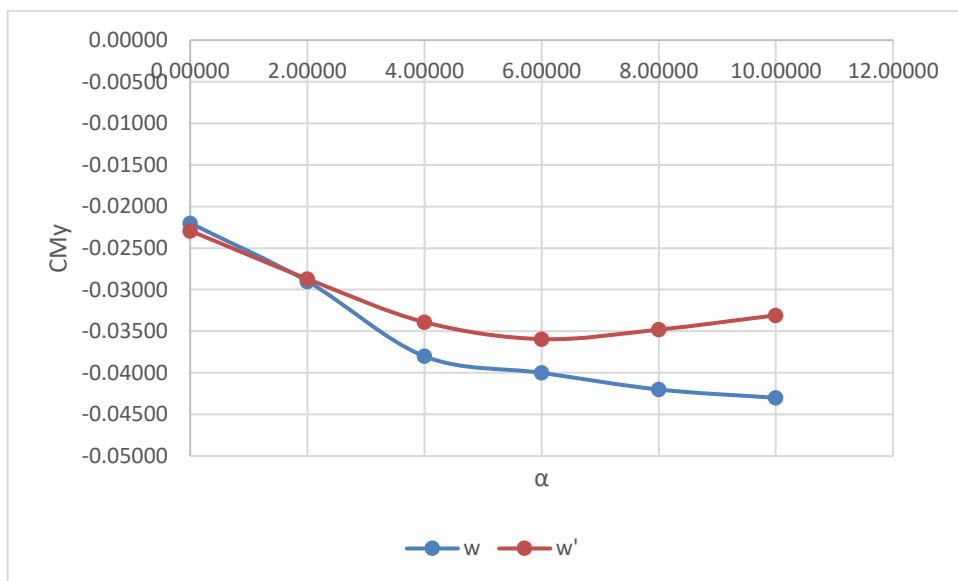


Figure 4. 11 CMY- α comparison curves

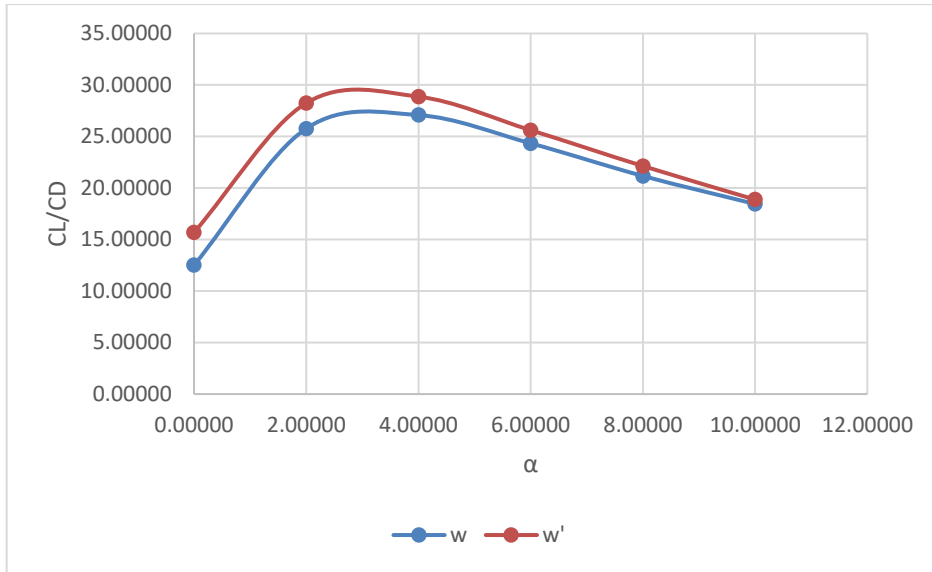


Figure 4.12 CL/CD- α comparison curves

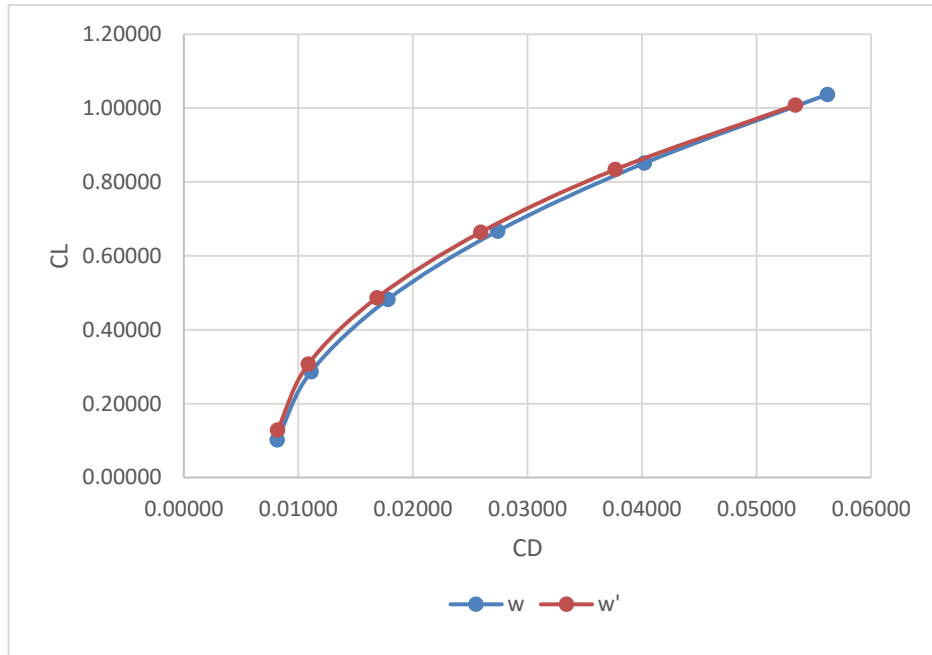


Figure 4.13 CL-CD comparison curves

4.6 Complete aircraft with different grid

Let's see the results with this grid on the complete aircraft (Table 4. 5):

AoA	CL	CDtot	CM _y	CL/CD
0.00000	0.12067	0.01079	-0.00053	11.18358
2.00000	0.31620	0.01365	-0.04957	23.16657
4.00000	0.51264	0.02057	-0.10090	24.91878
6.00000	0.70862	0.03139	-0.15365	22.57759
8.00000	0.89654	0.04563	-0.20345	19.64915
10.00000	1.08814	0.06446	-0.25140	16.88083

Table 4. 5 Complete aircraft tables of coefficient (new grid)

Opening the viewer of VSPAERO, we can also see the Delta Cp (Pressure coefficient change) gradient:

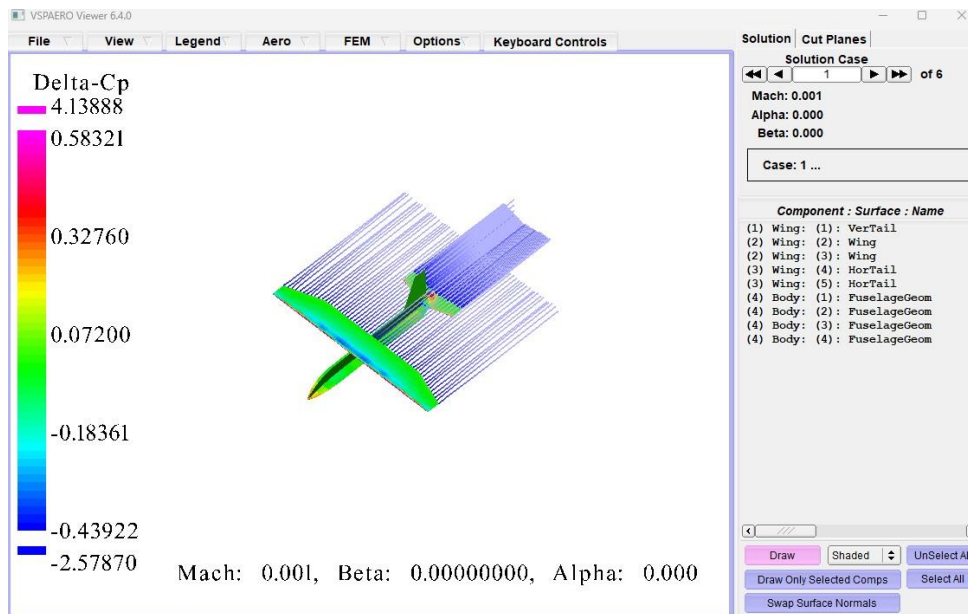


Figure 4. 14 VSP viewer: $\alpha=0$

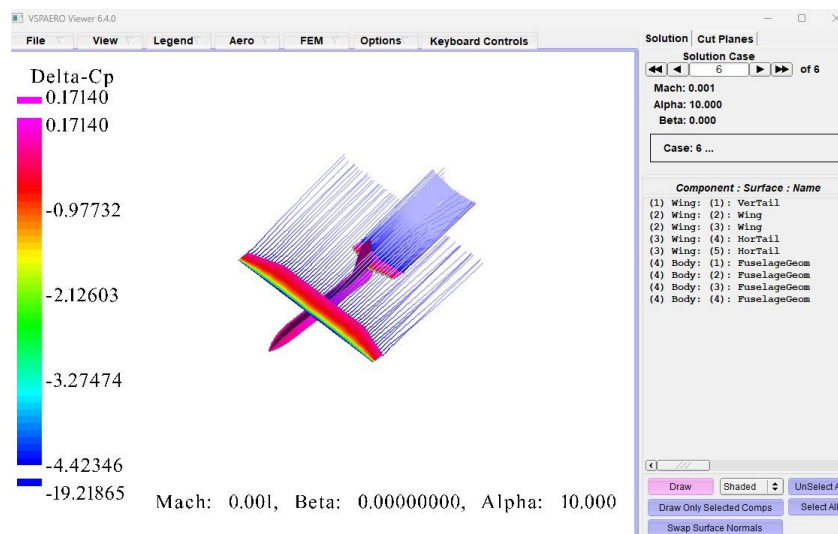


Figure 4. 15 VSP viewer: $\alpha = 10$

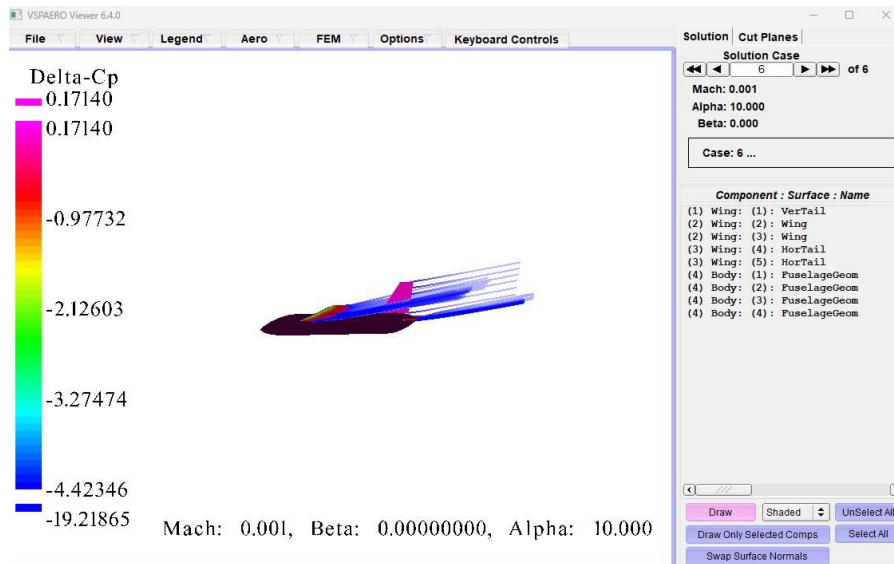


Figure 4. 16 $\alpha=10$ details

In the viewer, we can see also the direction of the rotation and plotting the trailing wakes (Figure 4. 17), it shows how the actuator disk influence the wake itself.

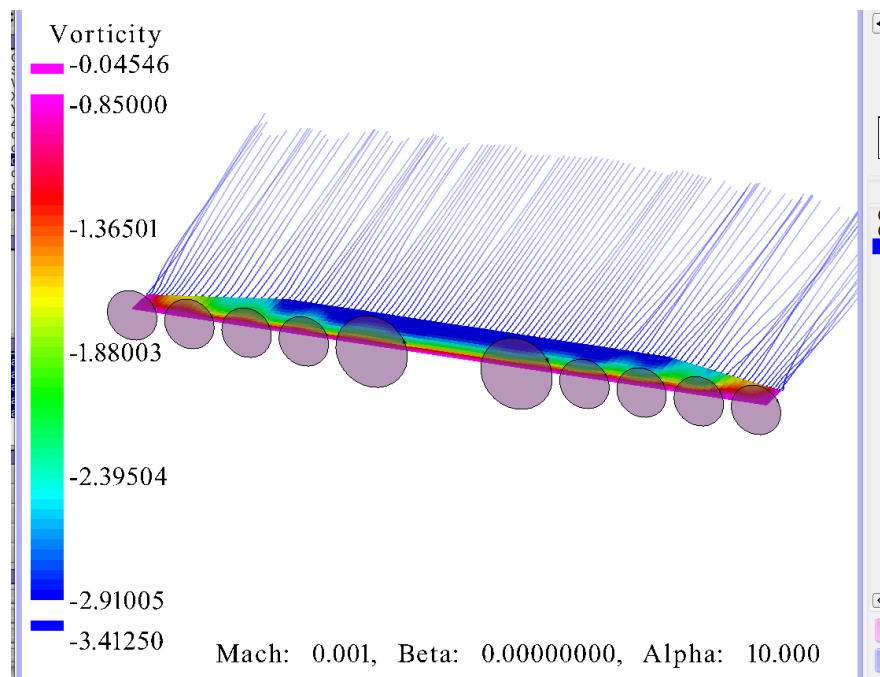


Figure 4. 17 Wakes with actuator disk model.

4.7 Flap effects

For this case, we have also studied what is the effect of flap deflection at 15° and 30° , by selecting the angles on the panel of VSPAERO shown in Figure 4. 18:



Figure 4. 18 Flap panel

If we compare the analyses with flaps deflection at 0°, 15°, 30°, we obtain:

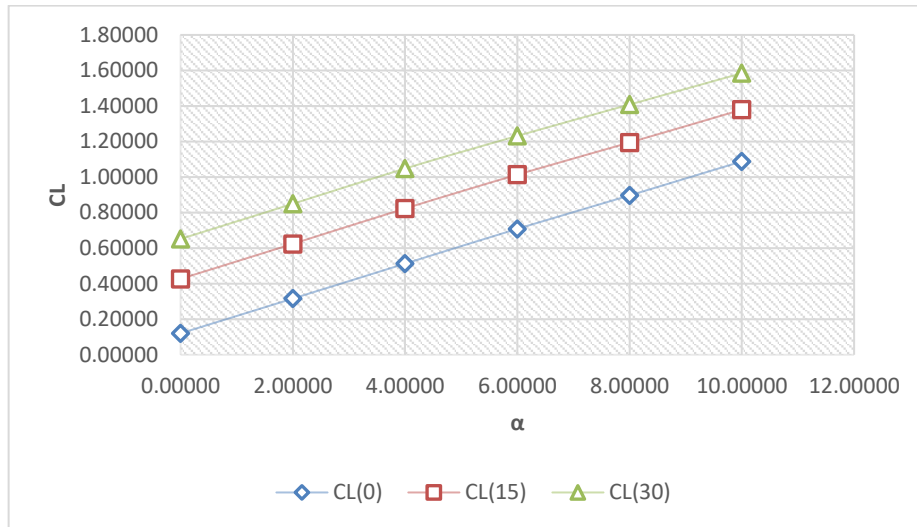


Figure 4. 19 CL- α deflections effects comparison plot

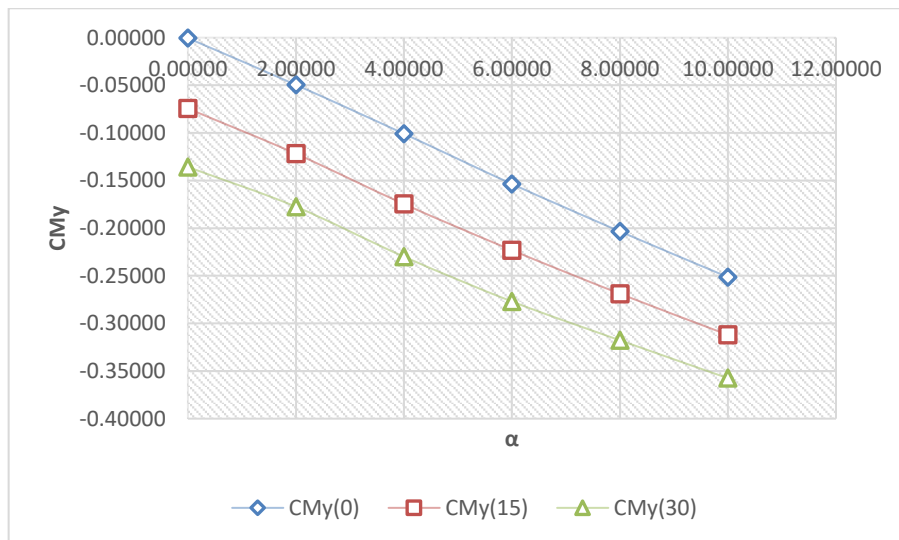


Figure 4. 20 CMy- α deflections effects comparison plot

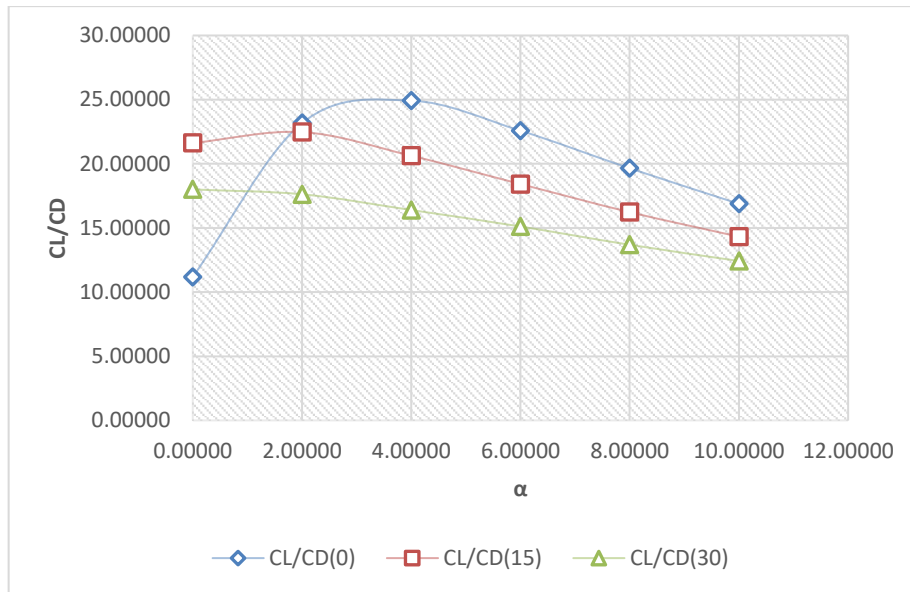


Figure 4. 21 CL/CD- α deflections effects comparison plot

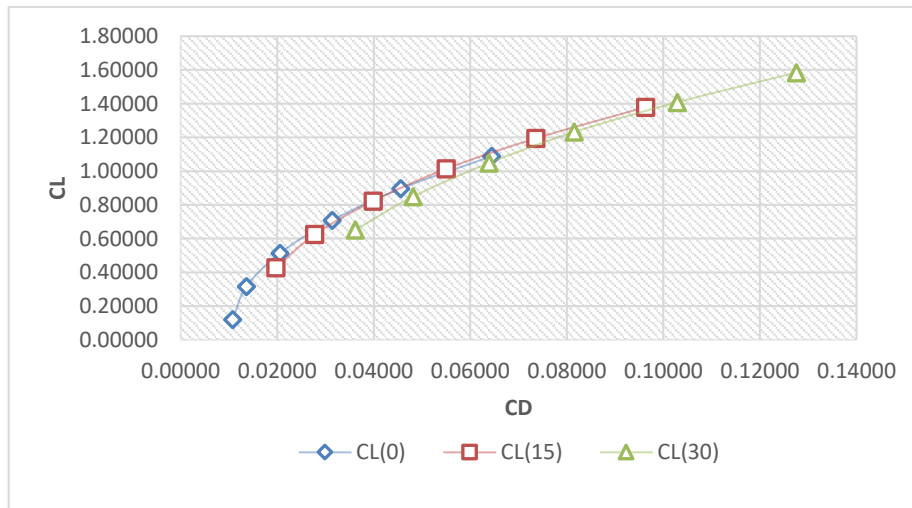


Figure 4. 22 CL-CD deflections effects comparison plot

Flaps curves move CL upward (Figure 4. 19), CM_y downward (Figure 4. 20) and CD to the right because it increases aerodynamic drag but VSPAERO sees only the induced one and not the parasitic one.

Opening the '.lod' file, we can also plot the aerodynamic load distribution for various angles of attack. It can be seen in Figure 4. 23:

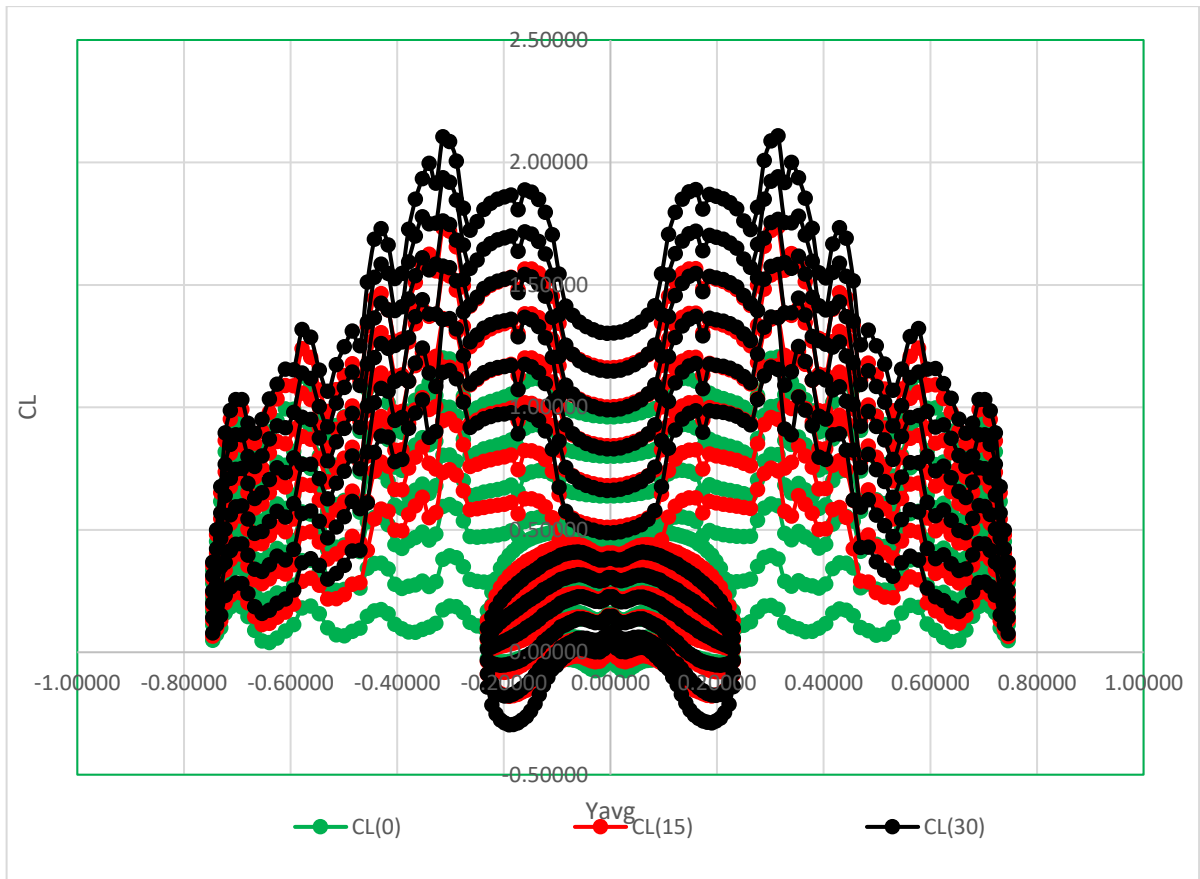


Figure 4. 23 Load distribution for various angles of attack

4.8 Elevator effects

Let's do the same analysis with different deflection of elevator (+10, -10, -20, -30) and flaps (15°, 30°), we can modify the deflection of this control surface on the same panel of flaps but adding a new control surface on the 'Control Grouping' section in Figure 4. 25:



Figure 4. 24 FLAP and ELEVATOR panel

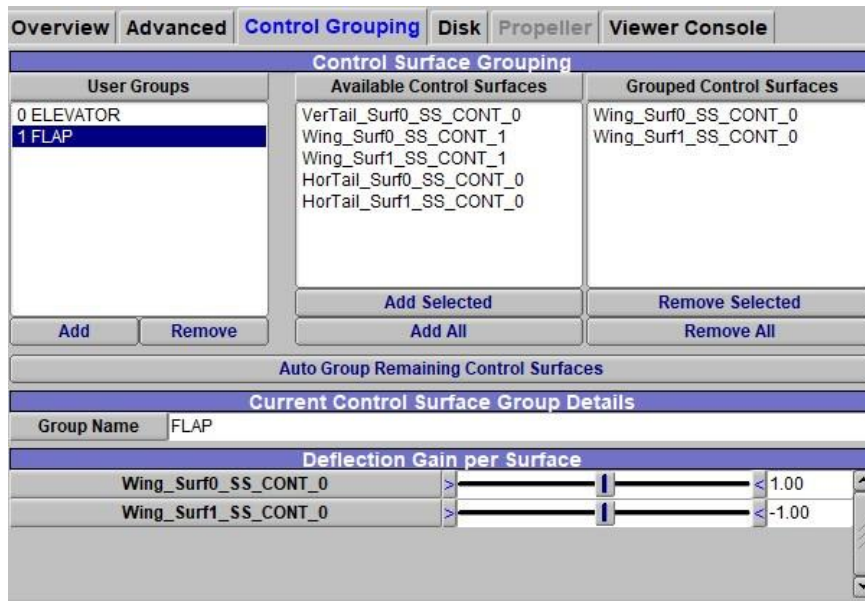


Figure 4. 25 Control Grouping section

Setting deflection of flaps at 0° , we obtain:

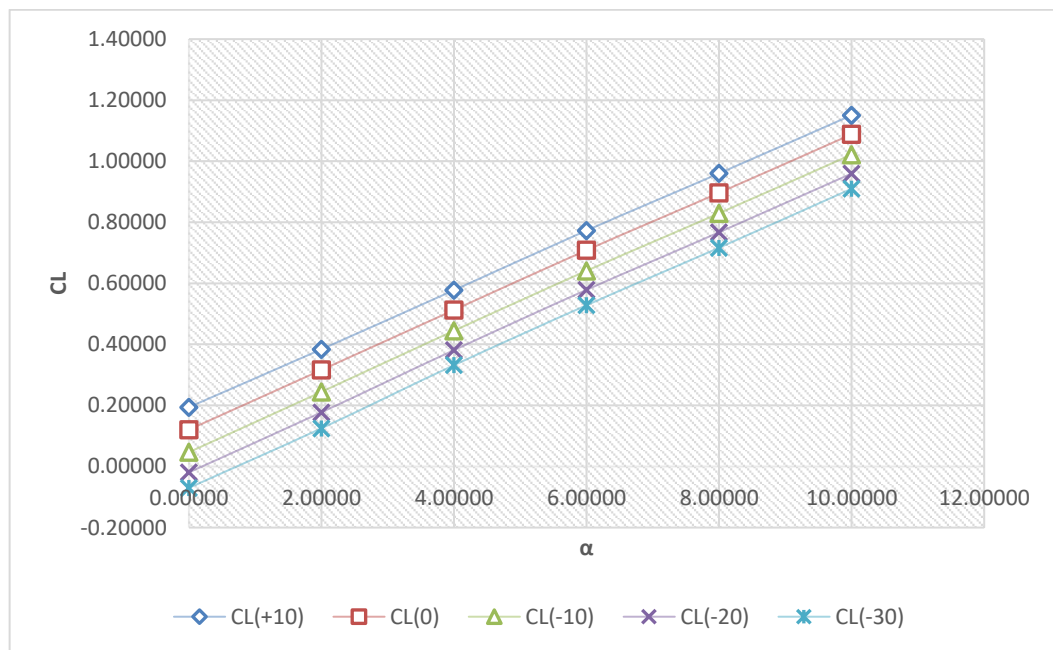


Figure 4. 26 CL- α at different deflection of elevator

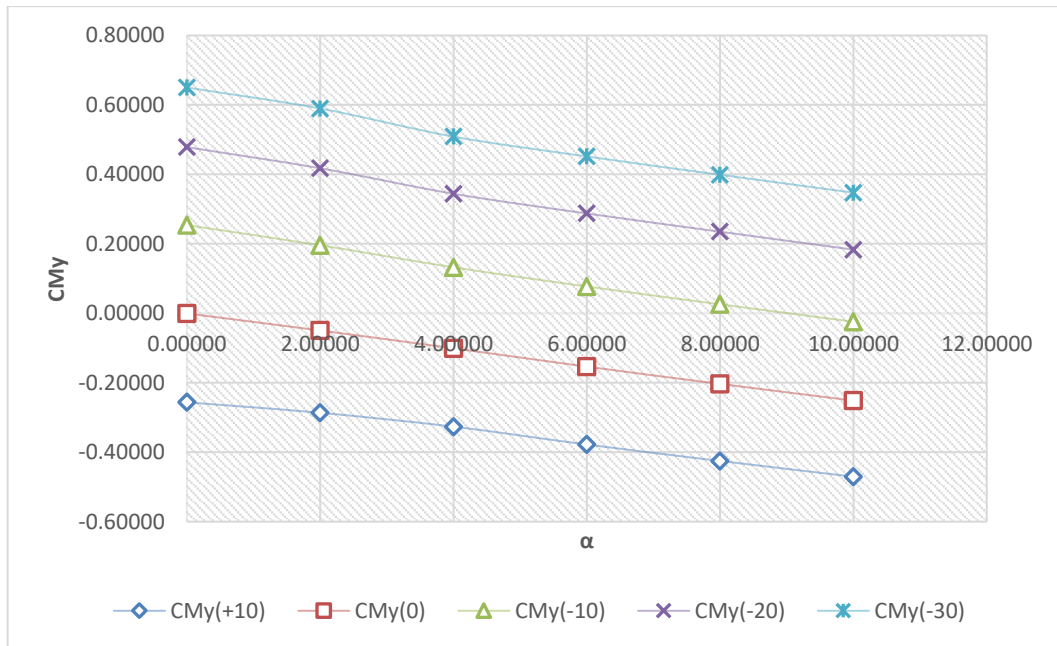


Figure 4.27 CM_y-α at different deflection of elevator

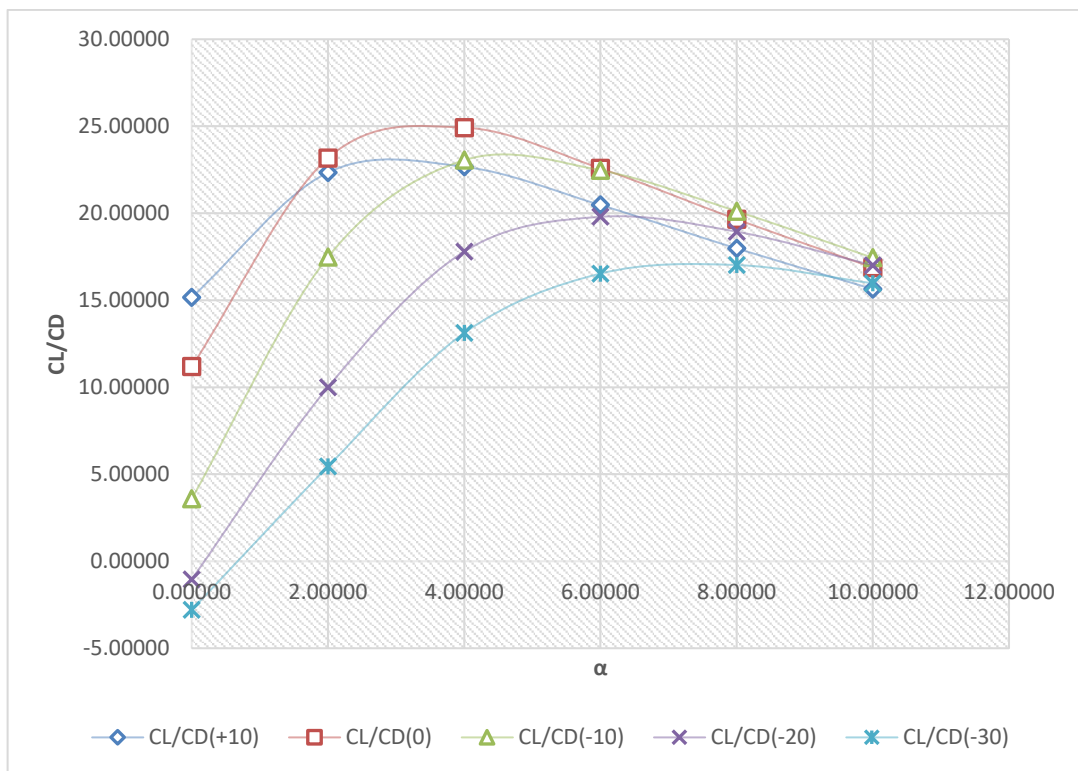


Figure 4.28 CL/CD-α at different deflection of elevator

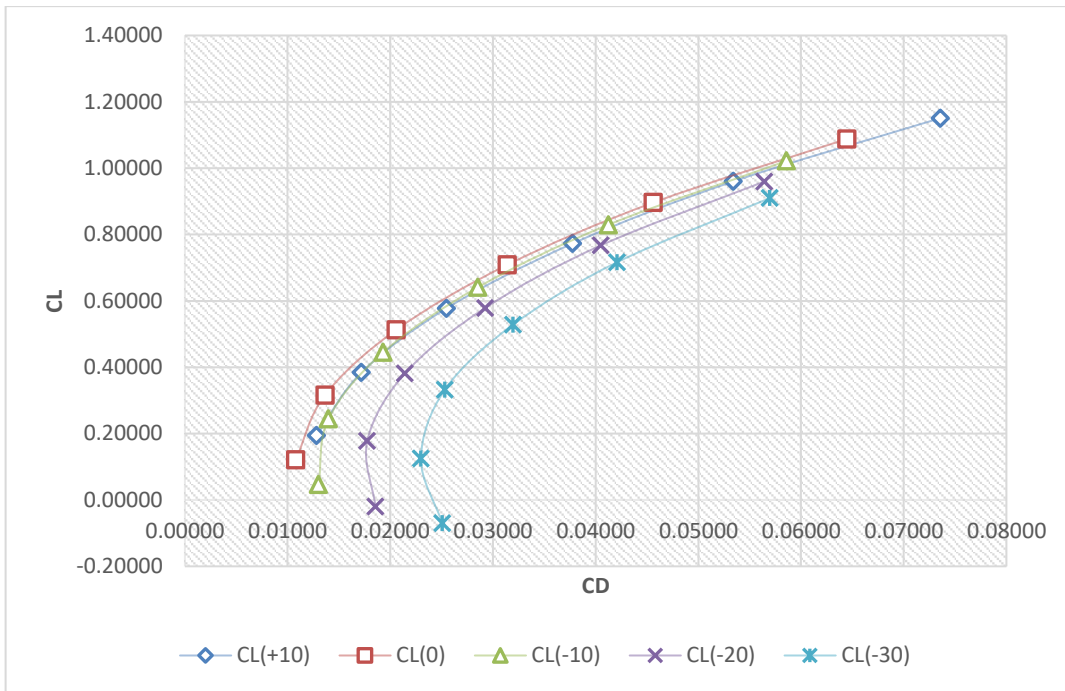


Figure 4. 29 CL-CD at different deflection of elevator

Setting flaps at 15°:

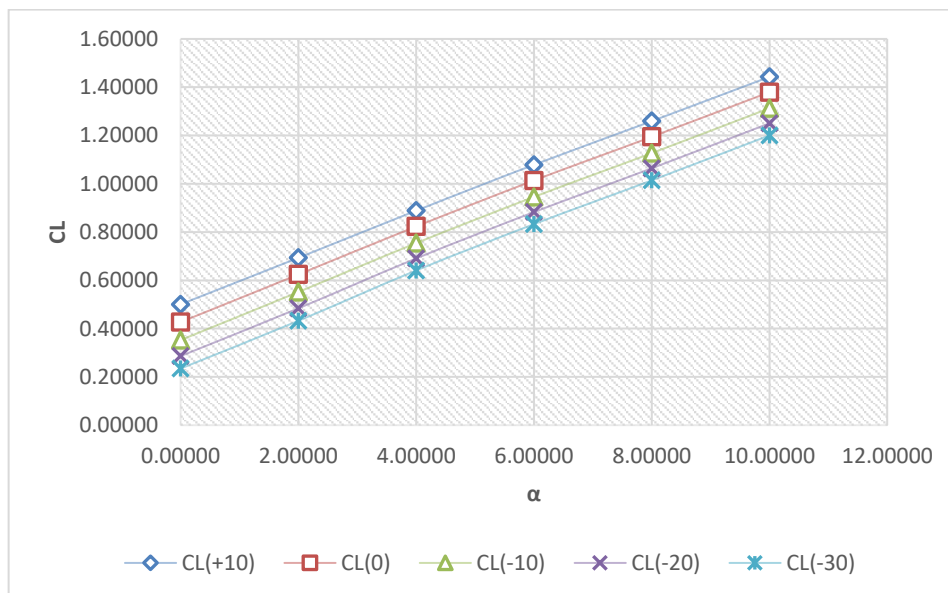


Figure 4. 30 CL-α at different deflection of elevator

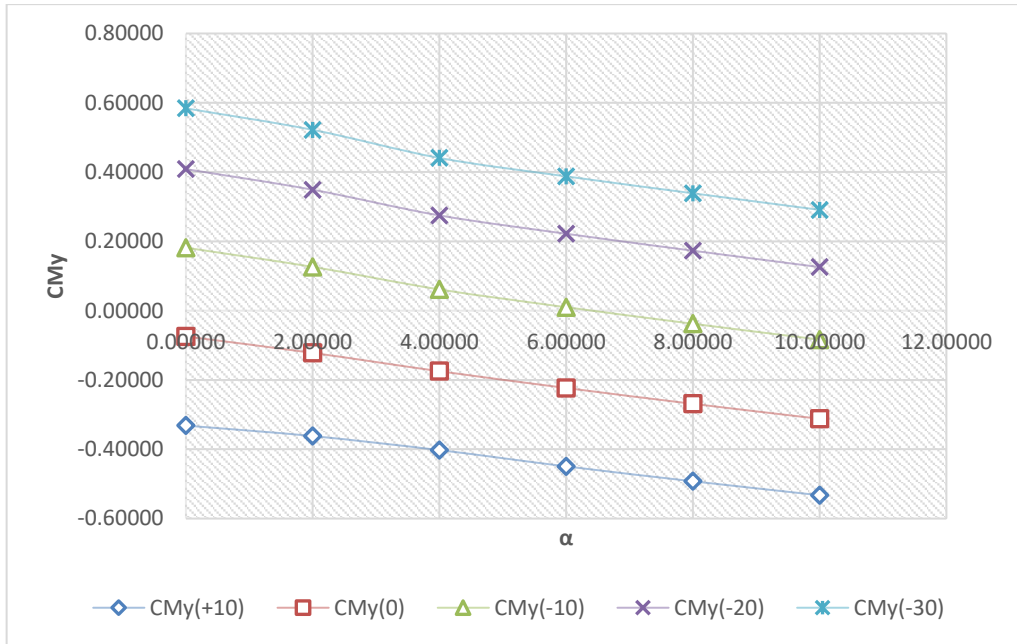


Figure 4.31 $CMY-\alpha$ at different deflection of elevator

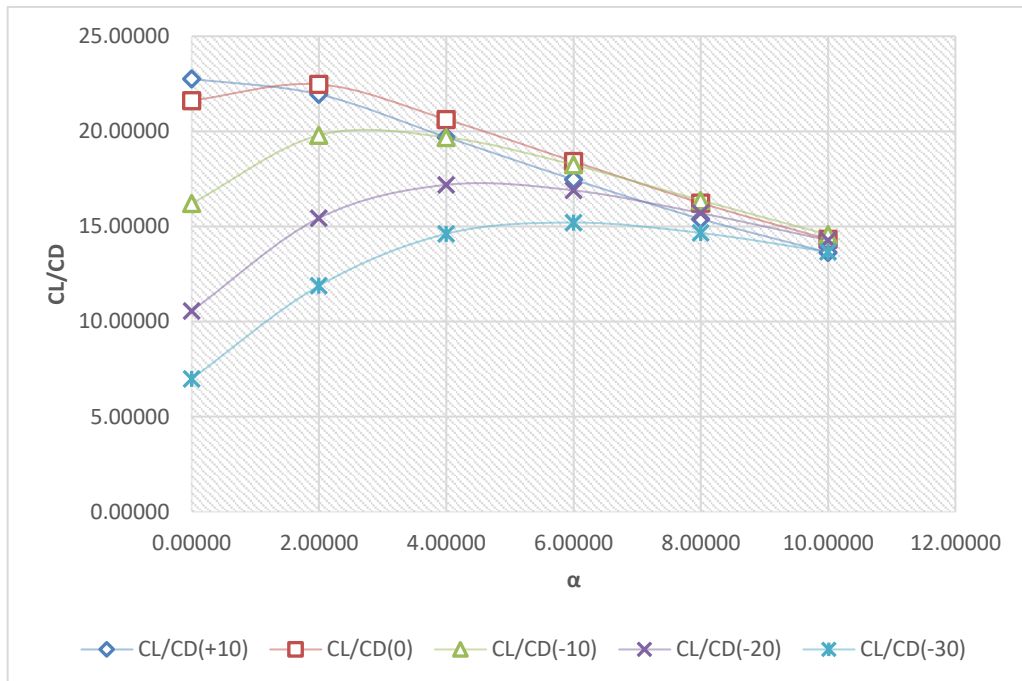


Figure 4.32 $CL/CD-\alpha$ at different deflection of elevator

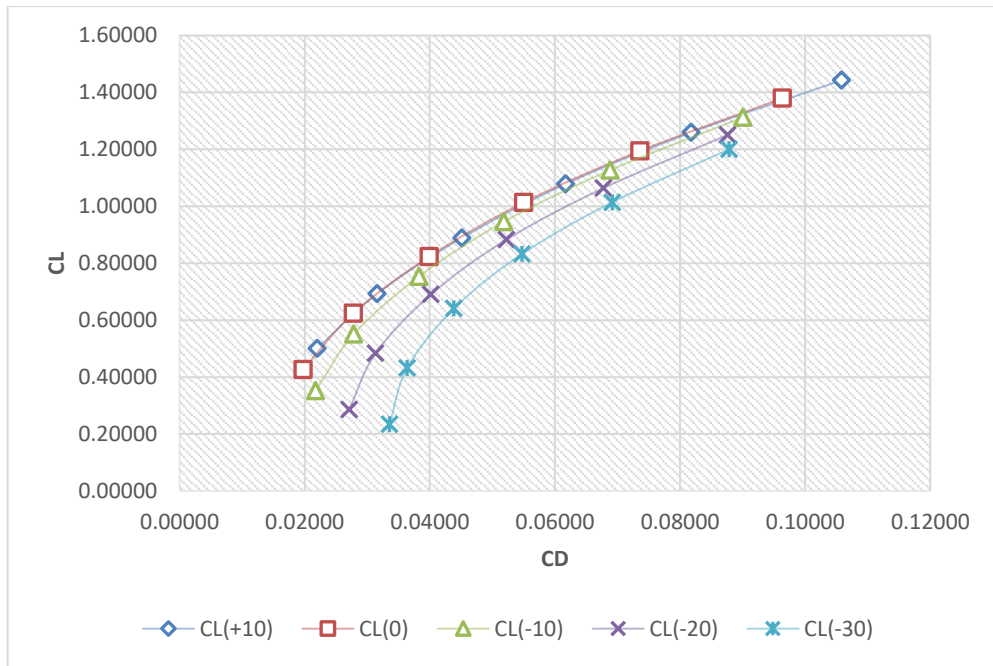


Figure 4.33 *CL-CD at different deflection of elevator*

With flaps at 30°, we have:

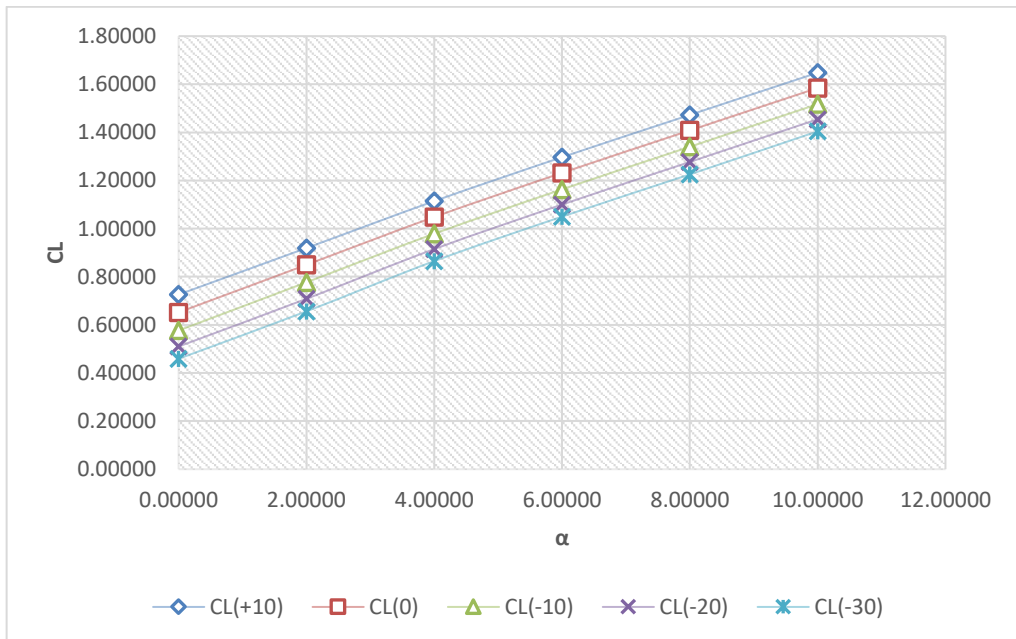


Figure 4.34 *CL-α at different deflection of elevator*

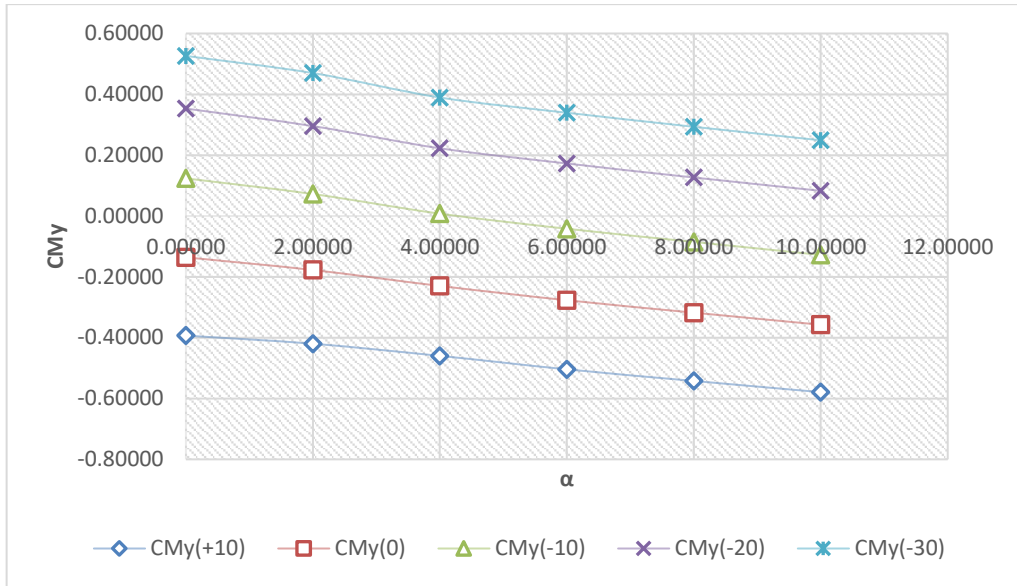


Figure 4.35 *CMY- α at different deflection of elevator*

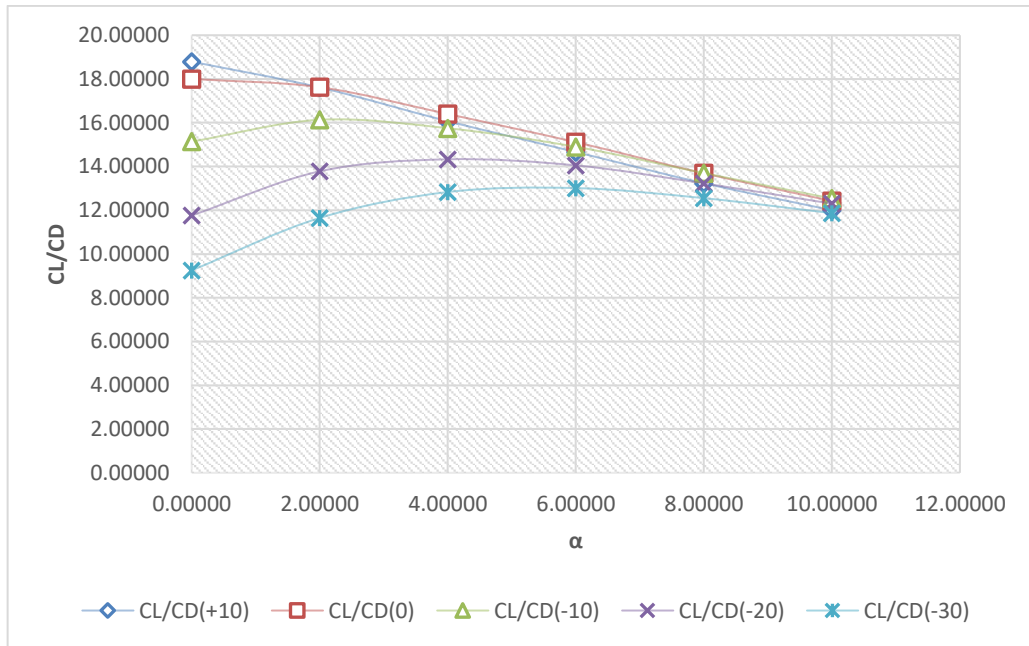


Figure 4.36 *CL/CD- α at different deflection of elevator*

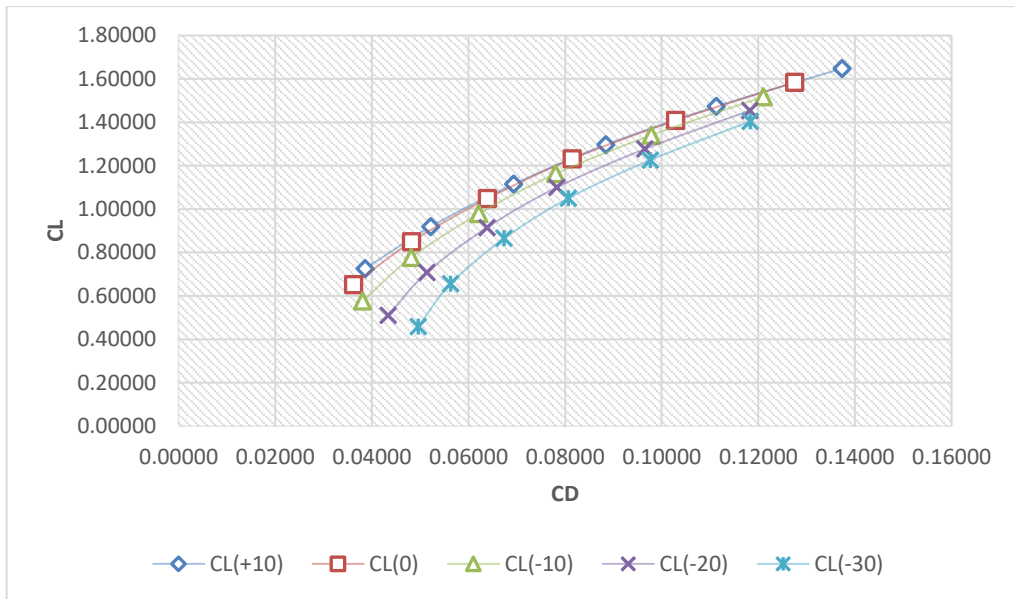


Figure 4.37 CL-CD at different deflection of elevator

4.9 Prop on- Prop off comparison

At the end of this work, we can show the difference between propellers on and propellers off to see the effects of DEP technology.

First, let's make a comparison of the global coefficient at different flaps deflections (0°-15°-30°):

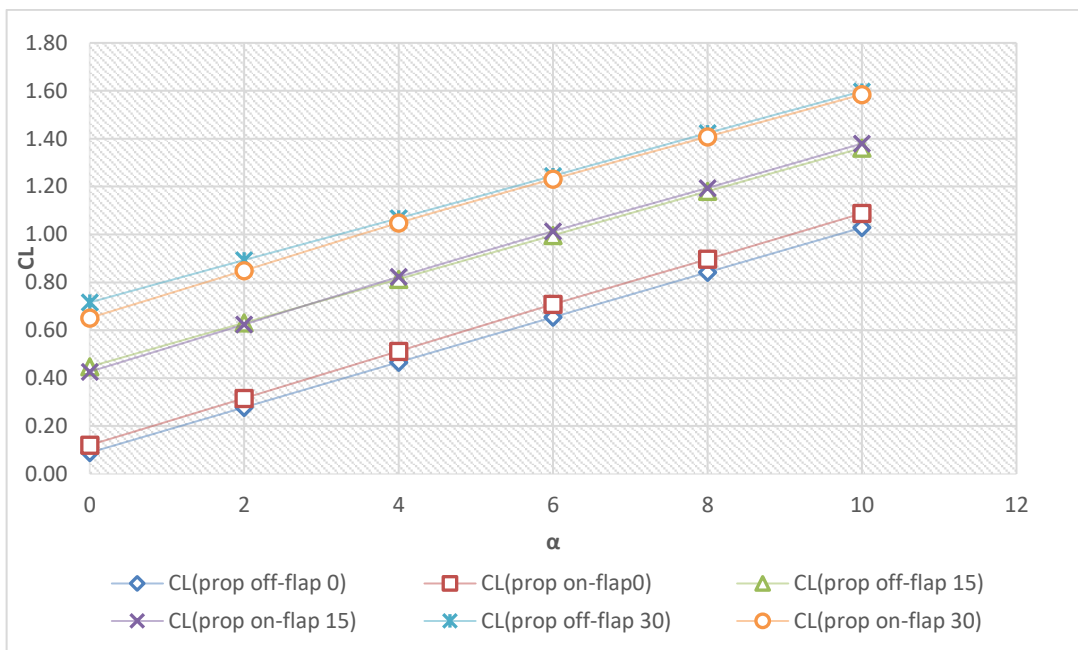


Figure 4.38 CL-a comparison plot

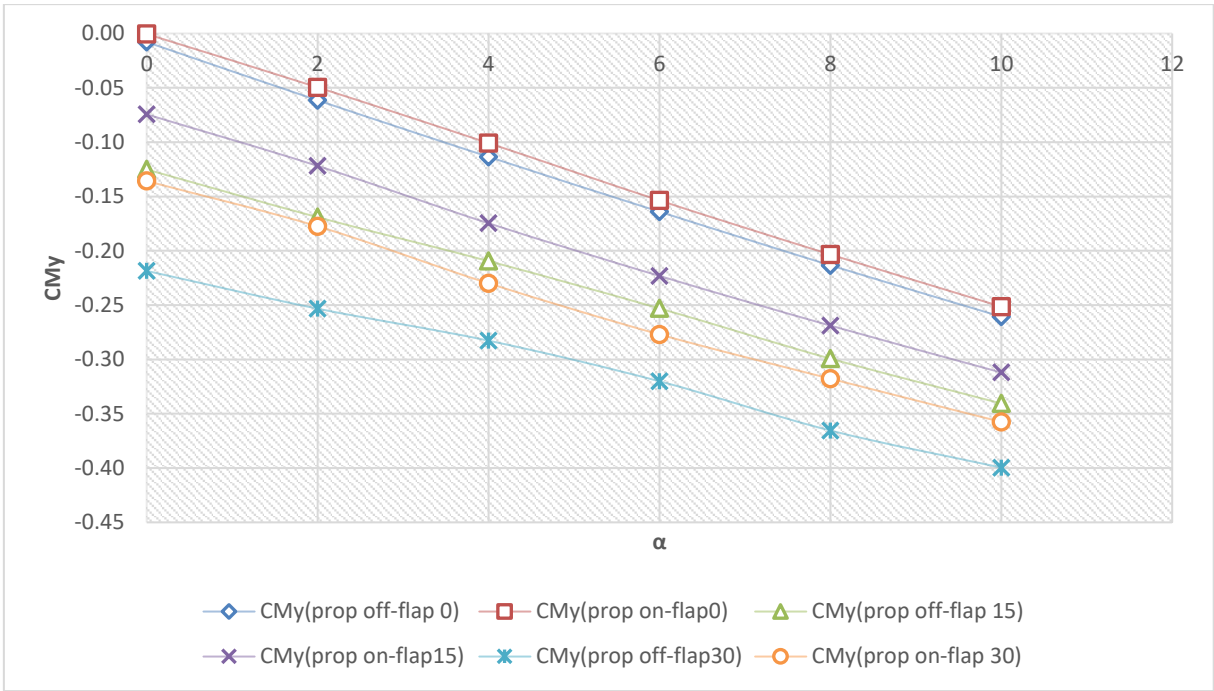


Figure 4.39 *CMY- α comparison plot*

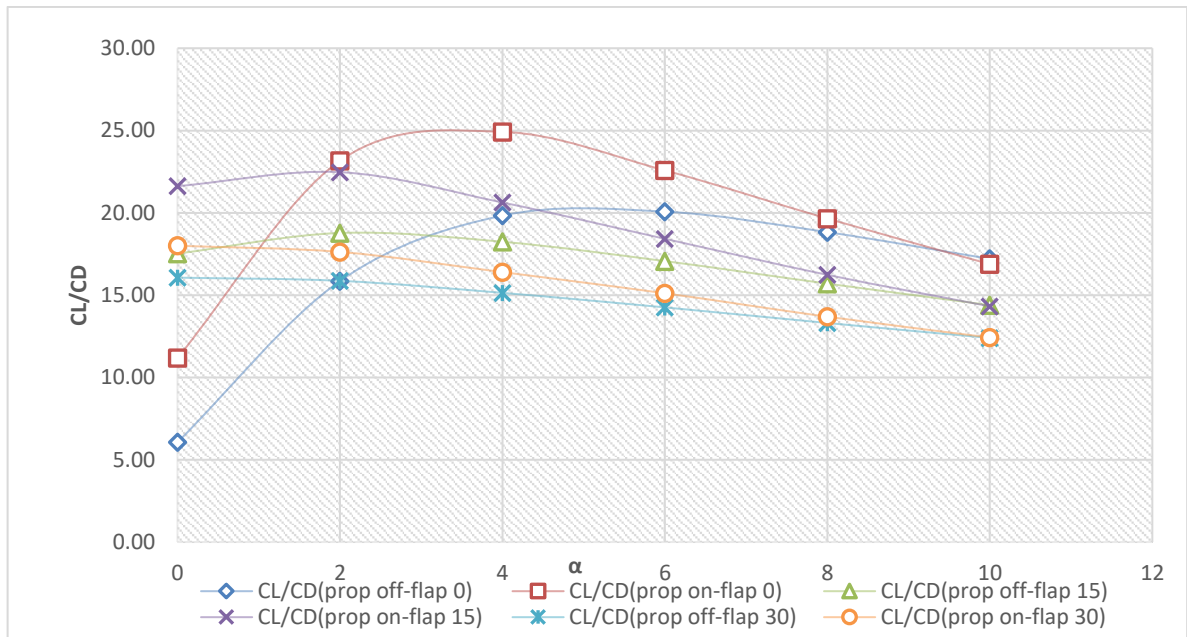


Figure 4.40 *CL/CD- α comparison plot*

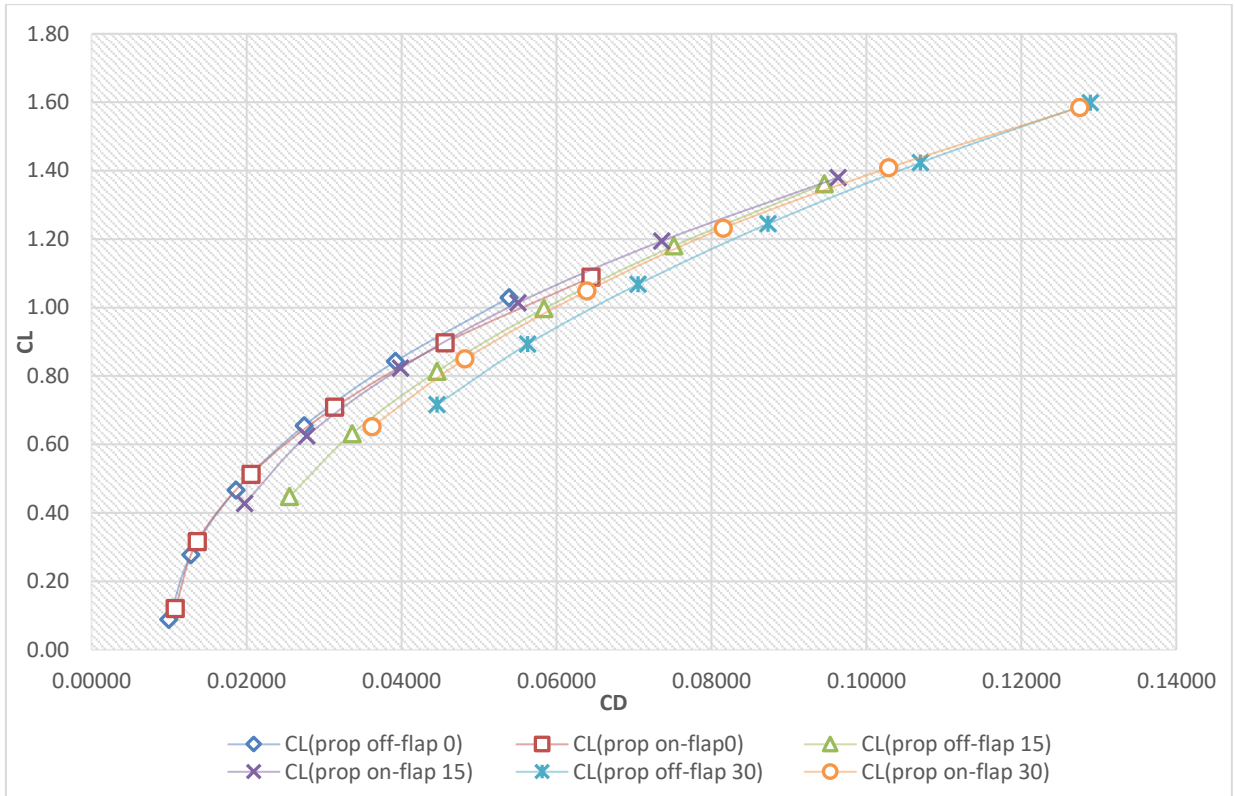


Figure 4. 41 CL-CD comparison plot

Then, we can compare aerodynamic load distribution at a certain angle of attack. In Figure 4. 42, we studied $\alpha=4$ at different deflection of flaps:

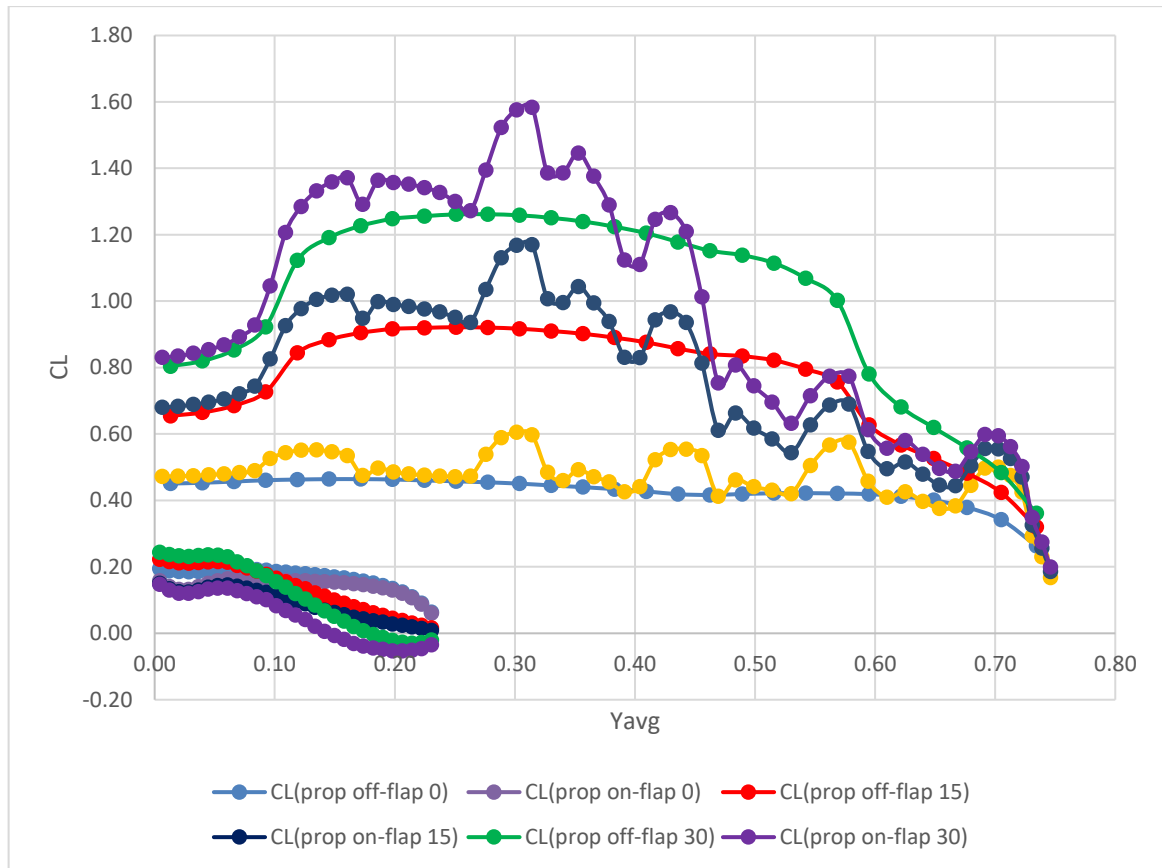


Figure 4.42 Load distribution comparison

As it was expected, the effect of this inboard-up propellers causes an increase of the lift coefficient that is more evident in the case where the deflection of the flaps is 0° , as it can be seen in Figure 4.38.

5. Conclusions

At the end of this thesis, it can be said that VSPAERO does a great job if we want the results of a first aerodynamic analysis. It has obviously some limitation, for example, as mentioned before, this tool does not see the parasitic drag, but only the induced one. Additionally, VSPAERO will not model separation of any kind, but it will help the user to find much of the aerodynamic traits of a model based on a given set of conditions. VSPAERO appears to be a linear and fast solver: it's not recommended for complex problems, but it is a great choice for models that require an approximate initial analysis.

Bibliography

- [1] Ambrosino, De Martino, “Aerodynamic analysis and surrogate modelling of distributed propulsion on commuter and regional aircraft through VLM and CFD methods”, 2019.
- [2] OpenVSP site: <https://openvsp.org/>.
- [3] VSPAERO Tutorial: <https://openvsp.org/wiki/doku.php?id=vspaerotutorial>.
- [4] The OpenVSP discussion group: <https://groups.google.com/g/openvsp>.
- [5] Hyun D. Kim; Aaron T. Perry; Phillip J. Ansell, “A Review of Distributed Electric Propulsion Concepts for Air Vehicle Technology”, 2018.
- [6] Nasti, “Modeling of a 19-pax scaled airplane model and preliminary evaluation of its stability and control characteristics”, 2022.
- [7] Nicholas K. Borer, Michael D. Patterson, Jeffrey K. Viken, Mark D. Moore, Joe Ben Bevirt, Alex M. Stoll and Andrew R. Gibson, “Design and Performance of the NASA SCEPTOR Distributed Electric Propulsion Flight Demonstrator”, 2016.
- [8] Nicholas K. Borer, Joseph M. Derlaga, Karen A. Deere, Melissa B. Carter, Sally Viken, Michael D. Patterson, Brandon Litherland and Alex Stoll, “Comparison of Aero-Propulsive Performance Predictions for Distributed Propulsion Configurations”, 2017.
- [9] Tognaccini, “Lezioni di aerodinamica dell’ala rotante”, 2014-2015.
